Article

Neuron

Differential Regulation of Evoked and Spontaneous Release by Presynaptic NMDA Receptors

Highlights

- PreNMDAR control of evoked, but not spontaneous, release depends on rate and Mg^{2+}
- To sustain rapid evoked release, preNMDARs regulate RRP replenishment rate
- PreNMDAR regulation of evoked, but not spontaneous, release relies on RIM1αβ
- PreNMDAR regulation of spontaneous, but not evoked, release depends on JNK2

Authors

Therése Abrahamsson,
Christina You Chien Chou, Si Ying Li, ...,
William Todd Farmer,
Keith Kazuo Murai,
Per Jesper Sjöström

Correspondence

jesper.sjostrom@mcgill.ca

In Brief

A long-standing question has been how presynaptic NMDA receptors influence high-frequency evoked neurotransmission but spontaneous release at low rates. Providing resolution, Abrahamsson et al. show that these receptors regulate evoked and spontaneous release via distinct RIM1αβ- and JNK2-dependent mechanisms, respectively.

Abrahamsson et al., 2017, Neuron *96*, 839–855
November 15, 2017 © 2017 Elsevier Inc.
https://doi.org/10.1016/j.neuron.2017.09.030

CellPress

Neuron
Article

Differential Regulation of Evoked and Spontaneous Release by Presynaptic NMDA Receptors

Therése Abrahamsson,[1] Christina You Chien Chou,[1,2] Si Ying Li,[1] Adamo Mancino,[1] Rui Ponte Costa,[3,4] Jennifer Anne Brock,[1,2] Erin Nuro,[1,2] Katherine Anne Buchanan,[4] Dale Elgar,[4] Arne Vladimir Blackman,[4] Adam Tudor-Jones,[4] Julia Oyrer,[4] William Todd Farmer,[1] Keith Kazuo Murai,[1] and Per Jesper Sjöström[1,5,*]

[1]Centre for Research in Neuroscience, Brain Repair and Integrative Neuroscience Programme, Department of Neurology and Neurosurgery, The Research Institute of the McGill University Health Centre, Montreal General Hospital, Montreal, QC H3G 1A4, Canada
[2]Integrated Program in Neuroscience, McGill University, 3801 University Street, Montreal, QC H3A 2B4, Canada
[3]Centre for Neural Circuits and Behaviour, University of Oxford, Oxford OX1 3SR, UK
[4]Department of Neuroscience, Physiology and Pharmacology, University College London, 21 University Street, London WC1E 6DE, UK
[5]Lead Contact
*Correspondence: jesper.sjostrom@mcgill.ca
https://doi.org/10.1016/j.neuron.2017.09.030

SUMMARY

Presynaptic NMDA receptors (preNMDARs) control synaptic release, but it is not well understood how. Rab3-interacting molecules (RIMs) provide scaffolding at presynaptic active zones and are involved in vesicle priming. Moreover, c-Jun N-terminal kinase (JNK) has been implicated in regulation of spontaneous release. We demonstrate that, at connected layer 5 pyramidal cell pairs of developing mouse visual cortex, Mg^{2+}-sensitive preNMDAR signaling upregulates replenishment of the readily releasable vesicle pool during high-frequency firing. In conditional RIM1αβ deletion mice, preNMDAR upregulation of vesicle replenishment was abolished, yet preNMDAR control of spontaneous release was unaffected. Conversely, JNK2 blockade prevented Mg^{2+}-insensitive preNMDAR signaling from regulating spontaneous release, but preNMDAR control of evoked release remained intact. We thus discovered that preNMDARs signal differentially to control evoked and spontaneous release by independent and non-overlapping mechanisms. Our findings suggest that preNMDARs may sometimes signal metabotropically and support the emerging principle that evoked and spontaneous release are distinct processes.

INTRODUCTION

As an action potential (AP) arrives at a presynaptic nerve terminal, it gates presynaptic voltage-dependent Ca^{2+} channels (VDCCs) to evoke the release of neurotransmitter by Ca^{2+}-dependent fusion of synaptic vesicles, resulting in excitatory postsynaptic potentials. These steps are thus essential for information transfer at the synapse (Südhof, 2012). However, neurotransmitter release also occurs spontaneously, resulting in postsynaptic miniature excitatory responses known as minis (Kavalali, 2015). Although evoked release and minis were initially thought to employ the same release machinery, recent work suggests that there are specific and distinct molecular machinery in the presynaptic terminal that regulate spontaneous and evoked release separately (Kavalali, 2015). However, precisely how spontaneous and evoked release are separately regulated remains unclear.

The NMDA-type receptor (NMDAR) is a nonspecific cationic ionotropic glutamate receptor (Paoletti et al., 2013). In the classical view, postsynaptic NMDARs act via Ca^{2+} to signal coincidence detection in Hebbian plasticity (Maheux et al., 2015). However, additional and more unconventional modes of NMDAR function have also consistently been reported (Banerjee et al., 2016; Duguid and Sjöström, 2006; Nabavi et al., 2013). For example, NMDARs are also found presynaptically in, e.g., cortex (Berretta and Jones, 1996; Sjöström et al., 2003), hippocampus (McGuinness et al., 2010), and cerebellum (Bidoret et al., 2009). The function of presynaptic NMDARs (preNMDARs) has been perplexing, as their presynaptic location prohibits a role in classical Hebbian coincidence detection (Duguid and Sjöström, 2006). PreNMDARs are thus thought to also serve other functional roles, such as in regulating presynaptic release (Banerjee et al., 2016). Indeed, we found that in layer 5 (L5) of developing mouse primary visual cortex, preNMDARs specifically upregulate neurotransmitter release at pyramidal cell (PC) synapses onto PCs and Martinotti cells, but not onto basket cells (Buchanan et al., 2012). This tight synapse-type-specific functionality suggests that preNMDAR control of synaptic release is important in developing microcircuits (Larsen and Sjöström, 2015). However, although preNMDARs have been studied for decades, the molecular pathways by which they act remain largely unknown (Banerjee et al., 2016). Because NMDARs are hotspots for synaptic pathologies, such as Alzheimer's disease, schizophrenia, and epilepsy (Paoletti et al., 2013), it is critically important to understand the signaling pathways by which they act.

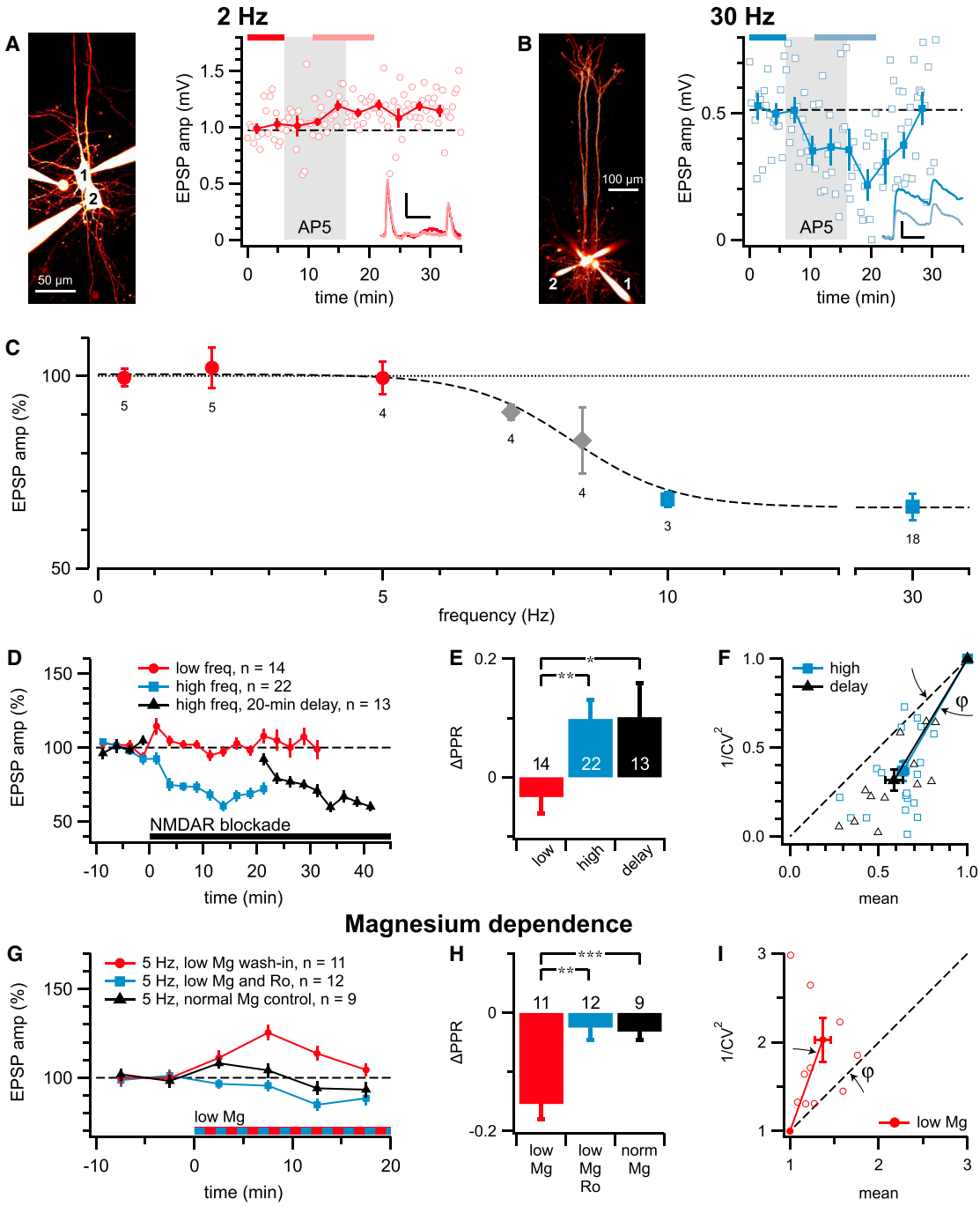

Figure 1. PreNMDAR Regulation of Evoked Release Depends on Frequency and Mg^{2+}

(A) Sample recording of monosynaptic connection from PC1 to PC2 showing that AP5 wash-in (gray box) did not suppress release at 2 Hz firing rate (before: 1.0 ± 0.03 mV, n = 22; after: 1.1 ± 0.02 mV, n = 31; upper tail: p = 0.99; two-tailed: p < 0.001, due to run-up). Open circles denote first EPSP in a train of five, and closed symbols show the same but averaged in ~3 min bins. Inset: first two EPSPs in a train of five indicated no change in short-term plasticity. Scale bars, 200 ms and 0.5 mV. Results are reported as mean ± SEM throughout, unless stated otherwise.

(B) AP5 wash-in reversibly reduced release at 30 Hz firing rate (PC1 to PC2, before: 0.52 ± 0.03 mV, n = 22; after: 0.30 ± 0.04 mV, n = 35; upper tail: p < 0.001; two-tailed: p < 0.001; symbols as in A). Inset: change in paired-pulse ratio suggested a presynaptic locus. Scale bars, 20 ms and 0.2 mV.

(C) PreNMDAR blockade reliably suppressed release at high, but not low, frequencies (normalized EPSP amplitude during drug at >8 Hz: 69% ± 3%, n = 25 of which n_{Ro} = 6 and n_{AP5} = 19, p < 0.001 versus 100%; at <8 Hz: 98% ± 2%, n = 18, p = 0.409 versus 100%; p < 0.001 for low versus high frequencies), consistent with the view that Mg^{2+}-blocked preNMDARs require sufficiently high firing rates to open but in apparent contradiction to the observation that low-frequency spontaneous release was downregulated (Figure 2). The x_{half} of numerically fit sigmoid (dashed) was 8.3 Hz. Digits under data points denote number of

(legend continued on next page)

Many presynaptic proteins have been implicated in the regulation of synaptic vesicle release. The Rab3-interacting molecules (RIMs) family of presynaptic proteins consists of seven members encoded by four genes: RIM1α and RIM1β; RIM2α, RIM2β, and RIM2γ; RIM3γ; and RIM4γ (Südhof, 2012). At the active zone, RIMs serve as central organizing scaffolding proteins that, e.g., recruit VDCCs, but they also act as signaling molecules in synaptic vesicle docking and priming and play a key role in neurotransmission (Castillo et al., 2002; Han et al., 2011; Kaeser et al., 2011; Schoch et al., 2002). Different RIM isoforms appear to perform similar and redundant roles in short-term plasticity (Kaeser et al., 2008b, 2011). RIM1α, however, is specifically required for presynaptic long-term plasticity in hippocampus and amygdala that can be mediated by retrograde endocannabinoid signaling (Castillo et al., 2002; Chevaleyre et al., 2007; Fourcaudot et al., 2008). Since cannabinoid-dependent presynaptic plasticity at connections between neocortical L5 PCs relies on preNMDARs (Sjöström et al., 2003), we hypothesized that preNMDARs may interact with RIM1 to regulate evoked glutamate release.

On the other hand, a recent study implicates C-Jun N-terminal kinases (JNKs) in preNMDAR-mediated regulation of spontaneous release (Nisticò et al., 2015). JNKs are serine-threonine kinases that belong to the mitogen-activated protein kinase (MAPK) family. There are three closely related vertebrate genes: JNK1 and JNK2 are ubiquitously expressed, whereas JNK3 is chiefly neuronal (Yamasaki et al., 2012). In brain development, JNKs are key regulators of, e.g., neuronal migration, dendrite formation, and axon maintenance (Yamasaki et al., 2012). Although JNK signaling is indispensable for preNMDAR-mediated regulation of spontaneous release in entorhinal cortex (Nisticò et al., 2015), it is unclear how JNKs relate to the regulation of evoked release, if at all.

Here, we aimed to elucidate the key signaling components of preNMDARs at excitatory connections onto L5 PCs. We found that preNMDARs signal via independent and non-overlapping pathways to control evoked and spontaneous release separately.

RESULTS

PreNMDAR Activation Is Frequency and Mg^{2+} Dependent

Previous studies in neocortex have shown that preNMDAR blockade downregulates evoked release (e.g., Brasier and Feldman, 2008; Buchanan et al., 2012; Sjöström et al., 2003). Since preNMDARs in L5 PCs are sensitive to the GluN2B-specific blocker Ro 25-6981 (Ro) (Buchanan et al., 2012), we hypothesized that they should be blocked by Mg^{2+} (Nabavi et al., 2013; Paoletti et al., 2013). If so, then preNMDAR blockade should only reduce neurotransmission at sufficiently high presynaptic AP frequencies, when preNMDARs are both glutamate bound and depolarized. To test this idea, we explored the frequency dependence of preNMDAR-dependent regulation of evoked release (Figure 1), using monosynaptically connected pairs of L5 PCs or extracellular stimulation (STAR Methods). In agreement, we found that AP5 or Ro only reduced neurotransmission above a critical presynaptic frequency of ~8.3 Hz (Figures 1A–1C).

In this view, the suppression of evoked neurotransmission by preNMDAR blockade is use dependent. To test this, we washed in Ro in the absence of spiking and found that—once spiking resumed—responses started at control rather than suppressed levels (Figure 1D). PreNMDAR-mediated regulation of neurotransmission thus depended on both usage and frequency.

To explore whether the suppression of neurotransmission was pre- or postsynaptically expressed, we analyzed the paired-pulse ratio (PPR) and the coefficient of variation (CV). Both approaches suggested a presynaptic locus of action (Figures 1E and 1F), in keeping with our previous studies (Buchanan et al., 2012; Sjöström et al., 2003).

We argued that if preNMDARs remain Mg^{2+} blocked below the critical frequency, then washing out Mg^{2+} should boost excitatory postsynaptic potentials (EPSPs) at rates below 8.3 Hz. In agreement, lowering Mg^{2+} from 1 to 0.2 mM during 5 Hz presynaptic spiking enhanced EPSP amplitude, but not in the presence of Ro (Figure 1G). This boosting was presynaptically expressed according to PPR and CV analyses (Figures 1H and 1I).

recordings. 23 of 43 recordings were carried out with extracellular stimulation (ES; STAR Methods), but this made no difference at low (ES 97% ± 2%, n = 12 versus paired 100% ± 5%, n = 6, p = 0.65) or high (ES 68% ± 4%, n = 11 versus paired 70% ± 4%, n = 14, p = 0.74) frequency. EPSP trains were evoked by 5 APs every 15–20 s or 1 AP every 10 s (for 0.1 Hz condition).

(D) Ensemble averages showed stability of low-frequency recordings (gray, 0.1–6 Hz) in the face of preNMDAR blockade as well as time course of suppression of neurotransmission in high-frequency recordings (red, 10–30 Hz). The suppression of release required presynaptic activity, as NMDAR blockade in the absence of spiking had no effect until 30 Hz bursts were resumed (blue; 59% ± 5%, n = 12, n_{Ro} = 6, n_{AP5} = 6; p < 0.001 versus 100%; p < 0.001 versus low frequency: 100% ± 2%; p = 0.839 versus high frequency: 63% ± 3%). Frequencies on the sigmoid slope (6–10 Hz) were omitted, and AP5 experiments were truncated before recovery, for clarity.

(E) PreNMDAR blockade reduced PPR after immediate (≥10 Hz, "high") or delayed ("delay") high-frequency firing, consistent with a presynaptic effect. However, PPR was unaffected at ≤6 Hz ("low," p = 0.253 versus zero), in agreement with preNMDARs upregulating release during high-frequency spiking.

(F) CV analysis resulted in points on or below the diagonal for high-frequency firing without (high; angle φ = 16° ± 2°, n = 21, p < 0.001) or with (delay; φ = 15° ± 2°, n = 13, p < 0.001) delay, which implies a reduced p_r. At low frequency, however, CV was not affected (−25° ± 20°, n = 14, p = 0.221; data not shown). Open symbols denote individual experiments.

(G) Below the critical frequency for preNMDAR activation (5 Hz, see C), reducing Mg^{2+} concentration from 1 to 0.2 mM boosted EPSP amplitude (red circles; 140% ± 9%) compared to controls (black triangles; 97% ± 8%, p < 0.01). This effect was abolished by Ro (blue squares; 90% ± 7%, p < 0.001 versus red circles), consistent with preNMDARs depending on Mg^{2+} to regulate evoked release. Because EPSP boosting decayed (red circles), we quantified boosting over a 6–15 min window centered on the peak.

(H) Mg^{2+}-dependent EPSP boosting altered the PPR in keeping with a presynaptic locus.

(I) CV analysis agreed that Mg^{2+}-dependent EPSP boosting was presynaptic (angle φ = 21° ± 5°, n = 11, p < 0.01). CV was not significantly affected in Ro (−13° ± 20°, n = 12, p = 0.53) or in controls (−49° ± 30°, n = 9, p = 0.11).

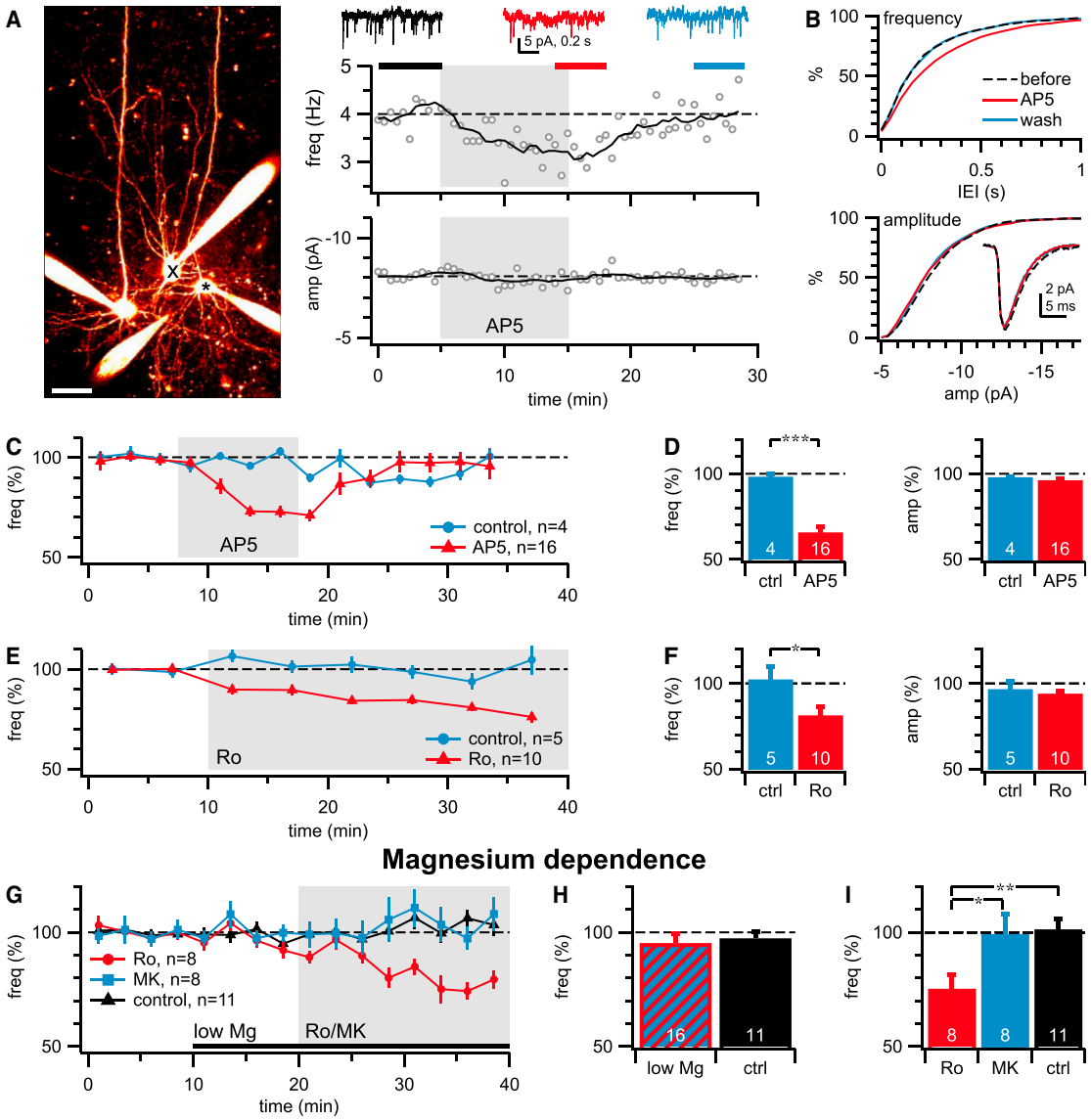

Figure 2. PreNMDAR Regulation of Spontaneous Release Does Not Depend on Mg^{2+}

(A) Sample L5 PC recording (asterisk) showed reversible reduction of mini frequency due to AP5 wash-in (top: red 3.2 ± 0.1 Hz versus black 4.1 ± 0.1 Hz, $p < 0.001$) but no effect on amplitude (bottom: red −8.0 ± 0.1 pA versus black −8.1 ± 0.06 pA, $p = 0.22$), indicating a presynaptic locus. Because AP5 wash-in is ineffectual in basket cells due to absence of preNMDARs (Buchanan et al., 2012), recorded neurons were carefully identified as PCs by 2PLSM (left: maximum-intensity projection of Alexa 594 fluorescence, STAR Methods; for comparison, note nearby basket cell labeled X lacking apical dendrite; scale bar represents 50 μm). Inset top: sample recording traces before (black), during (red), and after (blue) AP5.

(B) Cumulative frequency and amplitude histograms of minis acquired during periods indicated in (A). The absence of bimodality in the frequency histogram was consistent with all synaptic inputs being affected similarly by blockade. Inset bottom: average mini traces revealed no appreciable postsynaptic effect of AP5 wash-in (compare Figure S2).

(C) AP5 wash-in consistently reduced mini frequency reversibly (red) as compared to controls (blue). Baseline mini frequency was 3.3 ± 0.7 Hz, n = 20.

(D) Effect of AP5 wash-in on mini frequency was consistent but did not affect mini amplitude, in agreement with the existence of preNMDARs (Berretta and Jones, 1996; Sjöström et al., 2003).

(E) Wash-in of the GluN2B-specific blocker Ro 25-6981 (Ro) irreversibly reduced mini frequency (red) compared to controls (blue). Baseline mini frequency was 2.6 ± 0.3 Hz, n = 15.

(F) Ro wash-in consistently reduced mini frequency, but not amplitude, in agreement with these preNMDARs containing the GluN2B subunit (Brasier and Feldman, 2008; Sjöström et al., 2003; Woodhall et al., 2001).

(G) Mg^{2+} washout did not boost mini frequency (red/blue) compared to low Mg^{2+} controls (black), indicating that regulation of spontaneous release was Mg^{2+} independent (Nabavi et al., 2013). In agreement, wash-in of the channel pore blocker MK-801 (MK; blue) had no effect in low Mg^{2+}, yet the negative allosteric modulator Ro reduced mini frequency (red). Cells were loaded with internal MK-801 (STAR Methods) to block postsynaptic NMDAR ionotropic signaling.

(legend continued on next page)

In conclusion, Mg^{2+}-sensitive preNMDARs act as detectors of high-frequency presynaptic activity. During periods of high-frequency firing, preNMDARs may serve to boost evoked neurotransmission by upregulating release.

PreNMDAR Regulation of Spontaneous Release Does Not Depend on Mg^{2+}

The finding that preNMDAR blockade depends on frequency appeared to be at odds with prior findings that preNMDARs also regulate the rates of spontaneous release, which occurs well below 8.3 Hz in L5 PCs (Figure 1C) (Buchanan et al., 2012; Sjöström et al., 2003). We therefore revisited preNMDAR regulation of spontaneous release, recording minis in the presence of TTX and bicuculline (STAR Methods). To minimize postsynaptic NMDAR activation, we voltage clamped cells at −80 mV. In agreement with previous reports, we found that AP5 reduced mini frequency, but not amplitude (Figures 2A–2D), consistent with a presynaptic locus.

We were concerned that under potentially incomplete Mg^{2+} blockade, AP5 could possibly still act via postsynaptic NMDARs. Previous work in postnatal day 14 and 15 (P14 and P15) rats suggested that preNMDARs at connections onto L5 PCs contain the GluN2B subunit (Sjöström et al., 2003), when postsynaptic NMDARs have already undergone the GluN2B to GluN2A developmental switch (Stocca and Vicini, 1998). We therefore used the GluN2B-specific blocker Ro to avoid acting on postsynaptic NMDARs. In agreement with AP5 (Figures 2A–2D), we found a reduction in mini frequency, but not amplitude, due to Ro wash-in (Figures 2E and 2F), again suggesting a presynaptic locus.

However, the GluN2B to GluN2A developmental switch in neocortical L5 PCs was previously studied using evoked release in rats (Sjöström et al., 2003; Stocca and Vicini, 1998), whereas we studied spontaneous release in mice here. We therefore sought to verify this subunit switchover in mice with spontaneous release. We first validated that Ro could block postsynaptic NMDARs in young P3–P5 L5 PCs (Figure S1), before the GluN2B to GluN2A developmental switch (Stocca and Vicini, 1998). In addition to suppressing mini frequency, Ro reduced the NMDA:AMPA ratio at this young age, in keeping with postsynaptic NMDARs containing the GluN2B subunit at P3–P5 (Stocca and Vicini, 1998).

We next aimed to reproduce, in P11–P16 L5 PCs, the finding that presynaptic, but not postsynaptic, NMDARs are sensitive to GluN2B-specific blockade (Sjöström et al., 2003; Stocca and Vicini, 1998). We found that while AP5 wash-in reduced the frequency as well as the NMDA:AMPA ratio of minis, Ro selectively suppressed mini frequency but neither mini amplitude nor NMDA:AMPA ratio (Figure S2). Ro thus acts on pre-, but not post-, synaptic NMDARs in P11–P16 L5 PCs.

We wondered whether preNMDAR regulation of spontaneous release was Mg^{2+} independent and metabotropic (Nabavi et al., 2013). If so, Mg^{2+} wash-out should not enhance spontaneous release, even though this boosted evoked release (Figures 1G–1I). Indeed, washing out Mg^{2+} had no effect on mini frequency (Figures 2G and 2H) or amplitude (after/before low Mg: 99% ± 1%, n = 16 versus controls: 100% ± 1%, n = 11, p = 0.79). To block postsynaptic NMDARs, we hyperpolarized cells to −80 mV and dialyzed them with MK-801 (STAR Methods; Buchanan et al., 2012; Woodhall et al., 2001). If preNMDARs signal metabotropically to control spontaneous release (Nabavi et al., 2013), then Ro should reduce mini frequency, but the channel-pore blocker MK-801 should not, even in low Mg^{2+} (Reese and Kavalali, 2016). In agreement, Ro, but not MK-801, wash-in reduced spontaneous release rate (Figures 2G and 2I).

Taken together, these results verified, in mouse visual cortex L5 PCs, the finding that preNMDARs regulate spontaneous release rates (Berretta and Jones, 1996; Buchanan et al., 2012; Sjöström et al., 2003) and that these preNMDARs are sensitive to GluN2B-subunit-specific pharmacology (Brasier and Feldman, 2008; Sjöström et al., 2003; Woodhall et al., 2001). Additionally, our results indicated that preNMDARs regulating spontaneous release are not sensitive to Mg^{2+}, suggesting metabotropic signaling (Nabavi et al., 2013).

PreNMDARs Increase the RRP Replenishment Rate

We next investigated how preNMDARs regulate evoked release. Prior studies reported that preNMDAR blockade increased PPR (Brasier and Feldman, 2008; Buchanan et al., 2012; Sjöström et al., 2003) (also see Figure 1E), consistent with a reduction in the probability of synaptic release, p_r. It is possible, however, that a decreased p_r is secondary to reduced readily releasable pool (RRP) of vesicles or to a lowered RRP replenishment rate. To elucidate how preNMDARs control evoked release, we used the Schneggenburger-Meyer-Neher (SMN) approach (Schneggenburger et al., 1999) to explore what components of the presynaptic release machinery were affected by preNMDAR blockade. At the Calyx of Held, Schneggenburger et al. (1999) showed that a reduction of external Ca^{2+} concentration reduced RRP size without affecting replenishment rate. We first reproduced this finding at L5 PC-PC connections (Figures 3A, 3C, and 3D). Next, we washed in Ro while hyperpolarizing the postsynaptic cell to −90 mV (Figure 3B). With preNMDAR blockade, both RRP size and recovery rate were reduced, in stark contrast to the effect of Ca^{2+} reduction, which only reduced RRP size (Figures 3C and 3D).

The SMN approach comes with certain assumptions and pitfalls (Kaeser and Regehr, 2017; Neher, 2015). As an alternative, we tuned the Tsodyks-Markram (TM) model of short-term depression (Tsodyks and Markram, 1997) to our data using Bayesian inference (STAR Methods; Costa et al., 2013). We obtained results that were indistinguishable from the SMN approach—both Ca^{2+} reduction and Ro reduced the vesicle usage parameter U_{SE} of the TM model, but only Ro slowed down the recovery time constant $\tau_{recovery}$ (Figure S3). The TM

(H) Mg^{2+} washout had no effect on spontaneous release rates (red/blue in G pooled) compared to controls (black, p = 0.69) (Nabavi et al., 2013).
(I) Ro, but not MK, wash-in reduced mini frequency compared to controls. Mini amplitude remained indistinguishable (after/before Ro: 96% ± 2%, MK: 96% ± 2%, control: 99% ± 1%, p_{ANOVA} = 0.14, data not shown).
See also Figures S1 and S2.

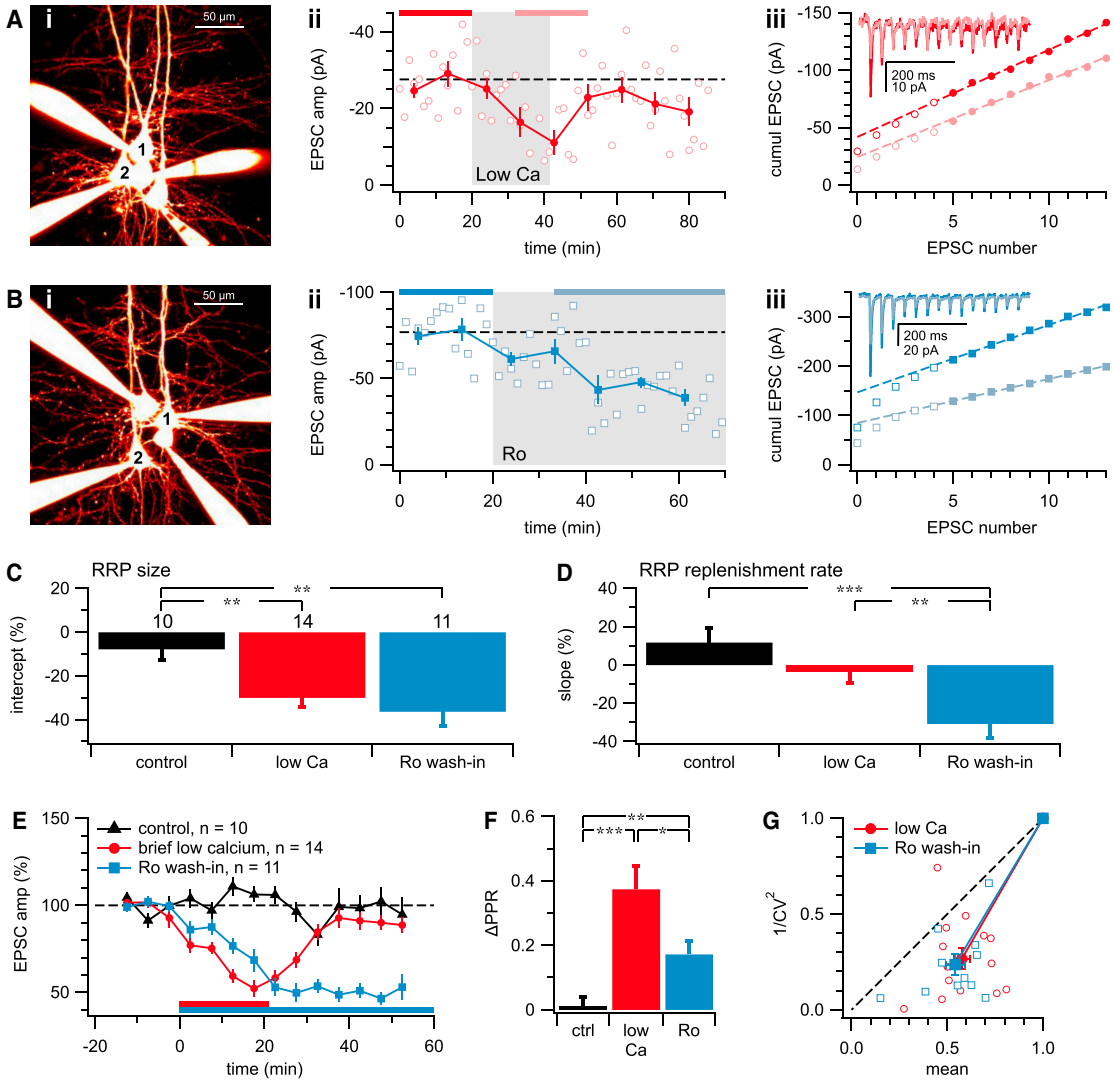

Figure 3. PreNMDARs May Regulate Evoked Release Indirectly by Controlling RRP Replenishment Rate

(A) Sample recording of connected PC pair (Ai: 1 to 2) for which reducing external Ca^{2+} concentration from 2 mM to 1 mM during 30 Hz firing reversibly reduced EPSC amplitude (Aii, red line: −28 ± 2 pA, n = 16; pink line: −14 ± 2 pA, n = 15; $p < 0.001$) and RRP size estimate (Aiii: y axis intercept of linear fit to cumulative responses), but not replenishment rate (Aiii: slope of linear fit), as previously shown at the Calyx of Held (Schneggenburger et al., 1999). Line was fit to steady state (closed symbols), thus avoiding initial curvature arising from RRP depletion (see Kaeser and Regehr, 2017; Neher, 2015). (Aiii), inset: 14 EPSCs at 30 Hz averaged over blue/red lines in (Aii).

(B) In contrast, at this sample connection from PC 1 to 2 (Bi), Ro wash-in irreversibly suppressed not only EPSC amplitude (Bii, blue line: −77 ± 4 pA, n = 16; pale blue line: −45 ± 4 pA, n = 35; $p < 0.001$) and RRP size measure (Biii: intercept), but also the RRP replenishment rate estimate (Biii: slope). (Biii), inset: EPSC averages, as in (Aiii).

(C) RRP size was robustly reduced by low Ca^{2+} or Ro wash-in compared to controls.

(D) Ro wash-in, but not low Ca^{2+}, consistently reduced the RRP replenishment rate, showing that preNMDAR signaling and Ca^{2+} influx do not have identical outcomes. Labels are as in (C).

(E) Ensemble averages showed stability of controls (black, 99% ± 3%, n = 10, p = 0.810 versus 100%), while briefly reducing Ca^{2+} from 2 mM to 1 mM (red, 58% ± 4%, n = 14, $p < 0.001$ versus controls) or Ro wash-in (blue, 54% ± 5%, n = 11, $p < 0.001$ versus controls, p = 0.596 versus Ca) both reliably suppressed EPSCs. Six of 14 Ca^{2+} reduction experiments were done with extracellular stimulation (STAR Methods) and the rest with paired recordings.

(F) PPR was as expected, unaffected in controls, but was increased by both Ca^{2+} reduction and Ro wash-in, consistent with reduced presynaptic release. The effect of low Ca^{2+} on PPR was stronger than that of Ro.

(G) CV analysis gave rise to points on or below the diagonal for Ca^{2+} reduction (red: 14° ± 4°, n = 14) and for Ro wash-in (blue: 15° ± 2°, n = 11, $p < 0.001$), consistent with a presynaptic locus. Controls were not systematically affected (36° ± 40°, n = 10, p = 0.441; data not shown).

See also Figure S3.

model fit thus corroborated our SMN method finding that preNMDARs act on RRP replenishment rate while Ca^{2+} does not.

We asked whether PPR and CV were affected in keeping with a presynaptic locus when probed with the SMN RRP depletion protocol, and we found that this was indeed the case (Figures 3E–3G). However, the effect of preNMDAR blockade on p_r may be secondary to a reduction in RRP replenishment rate.

Taken together, our findings indicate that—in evoked as opposed to spontaneous release—preNMDARs may serve to upregulate the RRP replenishment rate to maintain p_r during high-frequency firing, with possibly no direct effect on p_r itself.

PreNMDARs Are Unable to Regulate Evoked Release in RIM1 Deletion Mice

Presynaptic long-term plasticity at L5 PC-PC connections requires endocannabinoids and preNMDAR signaling (Sjöström et al., 2003), so we sought inspiration from similar forms of plasticity (Castillo et al., 2002; Chevaleyre et al., 2007; Fourcaudot et al., 2008), which implicated RIM1. To generate animals with RIM1$\alpha\beta$ conditionally knocked out (KO) hetero- or homozygously in neocortical excitatory neurons, we crossed RIM1$\alpha\beta^{fl/fl}$ (Kaeser et al., 2008b) and Emx1$^{Cre/Cre}$ (Gorski et al., 2002) mice (STAR Methods). We characterized neocortical RIM1 expression levels and found a stronger reduction in homo- compared to heterozygous RIM1$\alpha\beta$ KO mice (Figure S4A), without an effect on key synaptic proteins such as PSD95, vGlut1, GluN1, or GluN2B (Figure S4B). If preNMDARs rely on RIM1$\alpha\beta$ for signaling, then GluN2B-containing NMDARs and RIM1 might associate. Consistent with this, RIM1 co-immunoprecipitated with GluN2B (Figure S4C). Emx1$^{Cre/Cre}$ crossed with Ai9 expressed tdTomato in 90% of PCs (Figure S5; STAR Methods), verifying the high efficacy of Emx1$^{Cre/Cre}$ (Gorski et al., 2002).

We first explored the effect of preNMDAR blockade in RIM1$\alpha\beta^{fl/+}$;Emx1$^{Cre/+}$ KO mice, in which RIM1$\alpha\beta$ was conditionally deleted heterozygously (STAR Methods). To our surprise, the suppression of neurotransmission normally brought about by Ro-mediated preNMDAR blockade was abolished in Emx1$^{Cre/+}$;RIM1$\alpha\beta^{fl/+}$ mice, with no effect of Ro on RRP size estimate, RRP replenishment rate, EPSC amplitude, PPR, or CV (Figure 4). Suppression of neurotransmission in control RIM1$\alpha\beta^{fl/fl}$;no-Cre mice (Figure 4), however, was indistinguishable from that in wild-type (WT) mice (Figure 3). Postsynaptic cells were held at −90 mV. The robust obliteration of preNMDAR action in heterozygous Emx1$^{Cre/+}$;RIM1$\alpha\beta^{fl/+}$ KO mice suggested haploinsufficiency (Figure S4A).

We wondered what would happen to preNMDAR regulation of neurotransmission in homozygous RIM1$\alpha\beta$ KO mice. We compared current-clamp recordings of L5 PC-to-PC pairs in slices from Emx1$^{Cre/+}$;RIM1$\alpha\beta^{fl/fl}$ mice and from Emx1$^{Cre/+}$;RIM1$\alpha\beta^{+/+}$ littermates. As expected at resting membrane potentials in L5 PCs and in 1 mM Mg^{2+} (Markram et al., 1997), AP5 reduced the NMDA:AMPA ratio in PC-PC pairs (normalized ratio: 83% ± 4%, n = 23, $p < 0.001$ versus 100%) and thus considerably blocked postsynaptic NMDARs. Ro did not affect the NMDA:AMPA ratio (110% ± 8%, n = 7, $p = 0.28$ versus 100%, $p < 0.01$ versus AP5; Figure 5), suggesting no effect of Ro on postsynaptic NMDARs at this age (Figure S2) (Sjöström et al., 2003). However, there was no effect of either AP5 or Ro on EPSP amplitude, PPR, or CV in homozygous Emx1$^{Cre/+}$;RIM1$\alpha\beta^{fl/fl}$ KO mice (Figure 5), showing that, even though AP5 had an appreciable effect on postsynaptic NMDARs at resting membrane potential, there was no impact on presynaptic release. These findings further supported that presynaptic, but not postsynaptic, NMDARs need RIM1$\alpha\beta$ to regulate release.

To assess baseline neurotransmission, we retrospectively measured EPSP amplitude and PPR in nearly 400 paired L5 PC recordings in acute slices from Emx1$^{Cre/+}$;RIM1$\alpha\beta^{+/+}$, $^{fl/+}$, and $^{fl/fl}$ mice (Figure S6). We found that EPSPs were smaller and PPRs progressively larger in hetero- and homozygous KO animals, suggesting a lowered baseline p_r. This result verified that RIM1$\alpha\beta$ acts presynaptically on vesicle release (Südhof, 2012).

We conclude that preNMDARs critically depend on RIM1$\alpha\beta$ to upregulate the RRP during high-frequency firing and that conditional RIM1$\alpha\beta$ KO occludes the effects of preNMDAR blockade. This abolishment of preNMDAR signaling was indistinguishable in hetero- and homozygous RIM1$\alpha\beta$ KO mice, indicating haploinsufficiency.

RIM1 KO Reduces Axonal, but Not Dendritic, NMDAR-Mediated Ca^{2+} Supralinearities

RIM proteins play two key roles at the active zone: they scaffold and they mediate vesicle priming (Südhof, 2012). Our previous work revealed NMDA-mediated Ca^{2+} supralinearities in L5 PC boutons (Buchanan et al., 2012). We argued that, if the loss of preNMDAR function in RIM1$\alpha\beta$ KO mice was due to lack of preNMDAR scaffolding, then these Ca^{2+} supralinearities should be reduced or absent in mutant PC axons. If, however, the loss of function was due to a RIM1$\alpha\beta$ role in vesicle priming, then NMDA-mediated Ca^{2+} supralinearities may be entirely unaffected in RIM1$\alpha\beta$ KO PC axons. To explore these two possibilities, we photolyzed MNI-caged NMDA (MNI-NMDA) with brief 405 nm laser pulses and visualized Ca^{2+} supralinearities in L5 PC axons and dendrites with two-photon laser-scanning microscopy (2PLSM; see STAR Methods; Buchanan et al., 2012).

The existence of NMDAR-mediated supralinearities in dendritic compartments of principal excitatory neurons across the brain is well established (Maheux et al., 2015). With MNI-NMDA, we found robust Ca^{2+} supralinearities in L5 PC dendrites of Emx1$^{Cre/+}$;RIM1$\alpha\beta^{+/+}$, $^{fl/+}$, and $^{fl/fl}$ mice (Figures 6A–6F) (Buchanan et al., 2012), showing that RIM1 had no effect on postsynaptic NMDAR-mediated Ca^{2+} supralinearities. These supralinearities predictably vanished without MNI-NMDA. These results were expected from RIM1 being a classic presynaptic scaffolding and regulatory protein (Südhof, 2012) with no known postsynaptic location or function (Tang et al., 2016). We independently classified supralinear from linear Ca^{2+} signals using hierarchical clustering (Figure 6F) (STAR Methods; Buchanan et al., 2012).

When investigating L5 PC axonal compartments, we often found supralinearities in Emx1$^{Cre/+}$;RIM1$\alpha\beta^{+/+}$, $^{fl/+}$, and $^{fl/fl}$ mice that vanished when MNI-NMDA was removed (Figures 6G–6K), suggesting the existence of NMDARs close to synaptic terminals. In a subset of boutons, however, Ca^{2+} signals summed linearly and independently clustered with controls (Figure 6L), implying that some boutons did not have NMDARs, in agreement

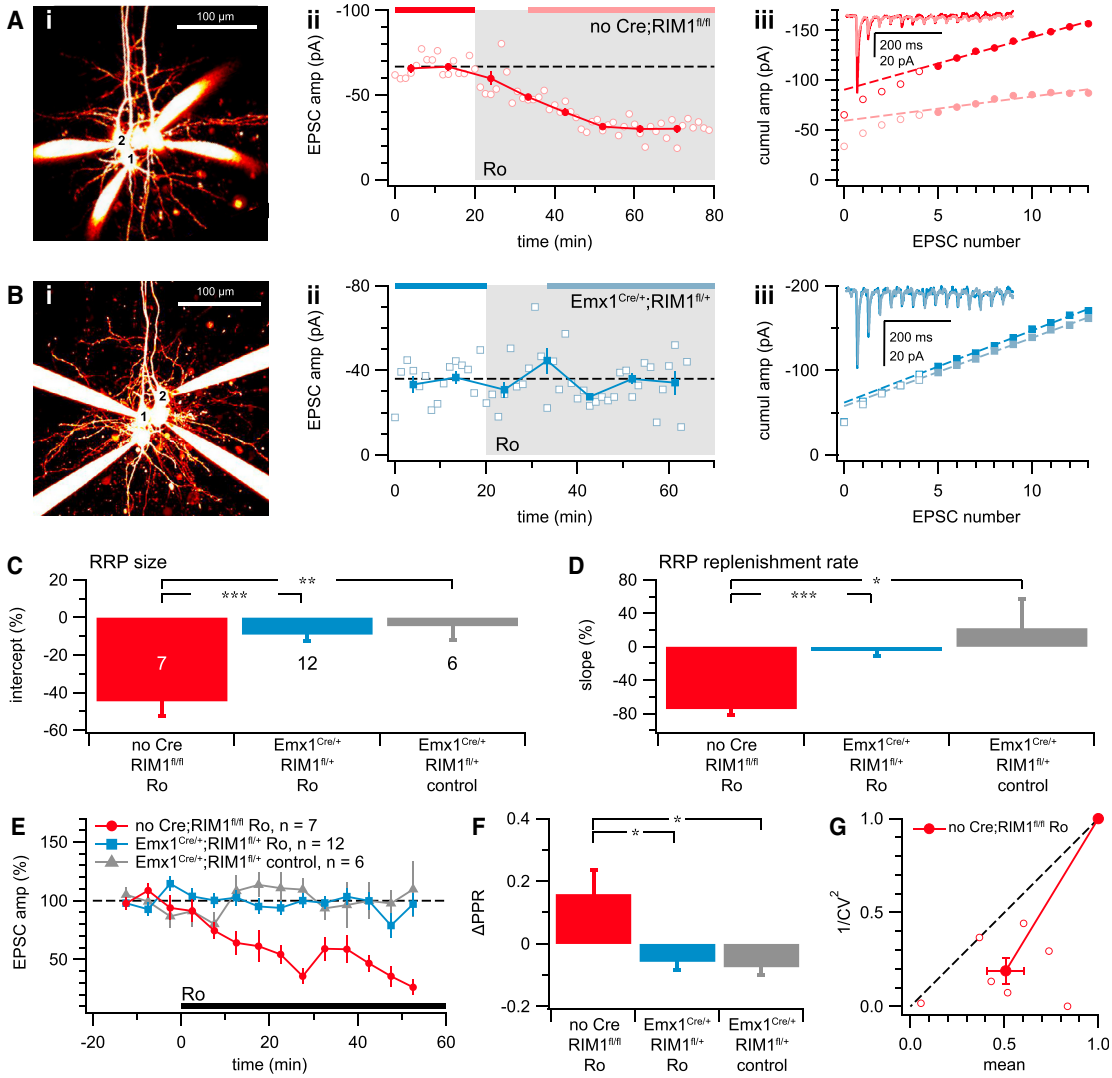

Figure 4. RIM1αβ Knockout Abolishes PreNMDAR-Dependent Regulation of Evoked Release

(A) Sample recording of unitary connection from PC 1 to 2 (Ai) showing that in no-Cre;RIM1αβ$^{fl/fl}$ controls, Ro wash-in reliably reduced EPSC amplitude (Aii, red: −67 ± 2 pA, n = 16; pink: −35 ± 1 pA, n = 35, p < 0.001), as well as RRP size and rate of replenishment (Aiii), just as in C57BL/6 mice (Figure 3).

(B) In this paired recording (Bi, 1 to 2) from a conditional heterozygous Emx1$^{Cre/+}$;RIM1αβ$^{fl/+}$ deletion animal, Ro did not affect EPSC amplitude (Bii, blue: −36 ± 2 pA, n = 16; pale blue: −33 ± 2 pA, n = 24, p = 0.43), RRP size, or recovery kinetics (Biii).

(C) Although Ro wash-in reliably reduced RRP size in no-Cre;RIM1αβ$^{fl/fl}$-positive controls (red), the change in RRP size in heterozygous Emx1$^{Cre/+}$;RIM1αβ$^{fl/+}$ KOs (blue) was indistinguishable from that in heterozygous Emx1$^{Cre/+}$;RIM1αβ$^{fl/+}$ deletion mock wash-in negative controls (gray).

(D) The RRP replenishment rate was reduced by Ro in no-Cre;RIM1αβ$^{fl/fl}$-positive controls (red), while in heterozygous Emx1$^{Cre/+}$;RIM1αβ$^{fl/+}$ KOs (blue), it was unaffected just like in heterozygous Emx1$^{Cre/+}$;RIM1αβ$^{fl/+}$ deletion mock wash-in controls (gray).

(E) After Ro wash-in, EPSC amplitude recorded in Emx1$^{Cre/+}$;RIM1αβ$^{fl/+}$ KOs (blue: 96% ± 4%, n = 12) was indistinguishable from that of Emx1$^{Cre/+}$;RIM1αβ$^{fl/+}$ mock wash-in controls (gray: 100% ± 10%, n = 6, p = 0.441 versus blue), suggesting a haploinsufficiency and a critical need for RIM1αβ in preNMDAR signaling. In no-Cre;RIM1αβ$^{fl/fl}$-positive controls, Ro wash-in led to a robust reduction of EPSC amplitude (red: 51% ± 10%, n = 7, p < 0.01 versus 100%, p < 0.01 versus gray, p < 0.001 versus blue), as expected.

(F) The PPR increase seen after Ro in no-Cre;RIM1αβ$^{fl/fl}$-positive controls (red) and C57BL/6 mice (Figures 1 and 3) was abolished in Emx1$^{Cre/+}$;RIM1αβ$^{fl/+}$ KOs (blue), leaving them indistinguishable from Emx1$^{Cre/+}$;RIM1αβ$^{fl/+}$-negative controls (gray), in keeping with a strong need for RIM1αβ in preNMDAR-dependent regulation of release.

(G) CV analysis indicated that Ro acted presynaptically in no-Cre;RIM1αβ$^{fl/fl}$-positive controls (14° ± 5°, n = 7, p < 0.05). CV was not systematically affected in Emx1$^{Cre/+}$;RIM1αβ$^{fl/+}$ KOs with Ro (37° ± 30°, n = 12, p = 0.254) or in Emx1$^{Cre/+}$;RIM1αβ$^{fl/+}$-negative controls (41° ± 50°, n = 5, p = 0.472).

See also Figures S4–S6.

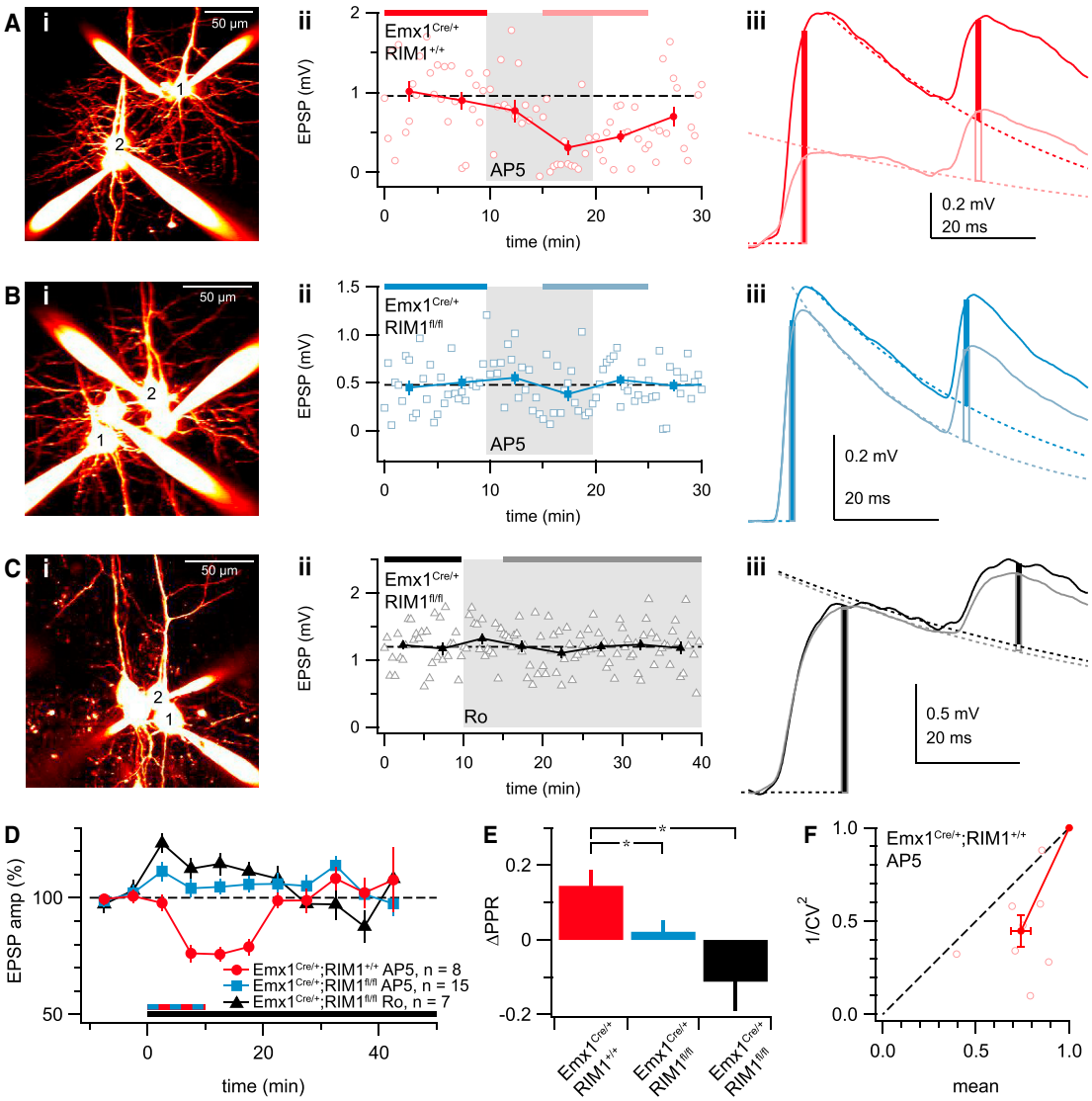

Figure 5. RIM1αβ Knockout Abolishes the Effects of Presynaptic, but Not of Postsynaptic, NMDAR Blockade

(A) Sample current-clamp recording of monosynaptic connection (Ai, PC 1 to 2) in acute slice from an Emx1$^{Cre/+}$;RIM1αβ$^{+/+}$ animal (STAR Methods), showing AP5-mediated downregulation of EPSP amplitude (Aii, red: 0.96 ± 0.09 mV, n = 31; pink: 0.38 ± 0.06 mV, n = 31, p < 0.001) and upregulation of PPR (Aiii), consistent with a reduction in p_r (Figures 1, 3, and 4). Dotted lines in (Aiii) are fitted exponentials used to account for temporal summation.

(B) In this paired recording (Bi, PC 1 to 2) from a conditional homozygous Emx1$^{Cre/+}$;RIM1αβ$^{fl/fl}$ KO slice, AP5 did not affect EPSP amplitude (Bii, blue: 0.48 ± 0.05, n = 31; pale blue: 0.46 ± 0.04, n = 31, p = 0.782) or PPR (Biii, note difference compared to Aiii). The windows for measuring EPSP amplitudes (blue open and closed bars) were set before peak EPSP to avoid measuring postsynaptic NMDAR component, which is appreciable at resting membrane potential (μ ± σ: −66 ± 0.4 mV over this recording) of L5 PCs (see Markram et al., 1997).

(C) In this paired recording (Ci, PC 1 to 2) from an Emx1$^{Cre/+}$;RIM1αβ$^{fl/fl}$ KO slice, Ro did not impact EPSP amplitude (Cii, black: 1.2 ± 0.06 mV, n = 31; gray: 1.2 ± 0.04 mV, n = 60, p = 0.79) or PPR (Ciii). Note that Ro wash-in did not affect the NMDA:AMPA ratio either (Ciii), as expected (Figure S2). Resting membrane potential was −64 ± 1 mV (μ ± σ).

(D) Although AP5 wash-in reversibly reduced EPSP amplitude in Emx1$^{Cre/+}$;RIM1αβ$^{+/+}$ PCs (red: 74% ± 6%, n = 8, p < 0.01 versus 100%), no effect of AP5 (blue: 100% ± 5%, n = 15, p < 0.001 versus red, p = 0.574 versus 100%) or Ro (black: 100% ± 6%, n = 7, p < 0.01 versus red, p = 0.533 versus 100%, p = 0.882 versus blue) was observed in PC recordings from Emx1$^{Cre/+}$;RIM1αβ$^{fl/fl}$ littermates, showing that preNMDAR-mediated regulation of release is abolished after homozygous RIM1 KO, as in heterozygotes (Figure 4). Resting membrane potential across pre- and postsynaptic L5 PCs was −65 ± 0.9 mV, n = 60.

(E) PPR was increased after AP5 in Emx1$^{Cre/+}$;RIM1αβ$^{+/+}$ controls (red). In Emx1$^{Cre/+}$;RIM1αβ$^{fl/fl}$ KOs, however, PPR was unaffected by AP5 (blue) or Ro (black), demonstrating a need for RIM1αβ in regulation of release.

(F) For Emx1$^{Cre/+}$;RIM1αβ$^{+/+}$ PCs, CV analysis gave rise to data points below the diagonal (18° ± 5°, n = 8, p < 0.05), suggesting a downregulation of p_r. For Emx1$^{Cre/+}$;RIM1αβ$^{+/+}$ PCs, however, CV was not consistently affected by AP5 (−7° ± 16°, n = 15, p = 0.61; data not shown) or by Ro (−24° ± 30°, n = 7, p = 0.51; data not shown).

See also Figure S6.

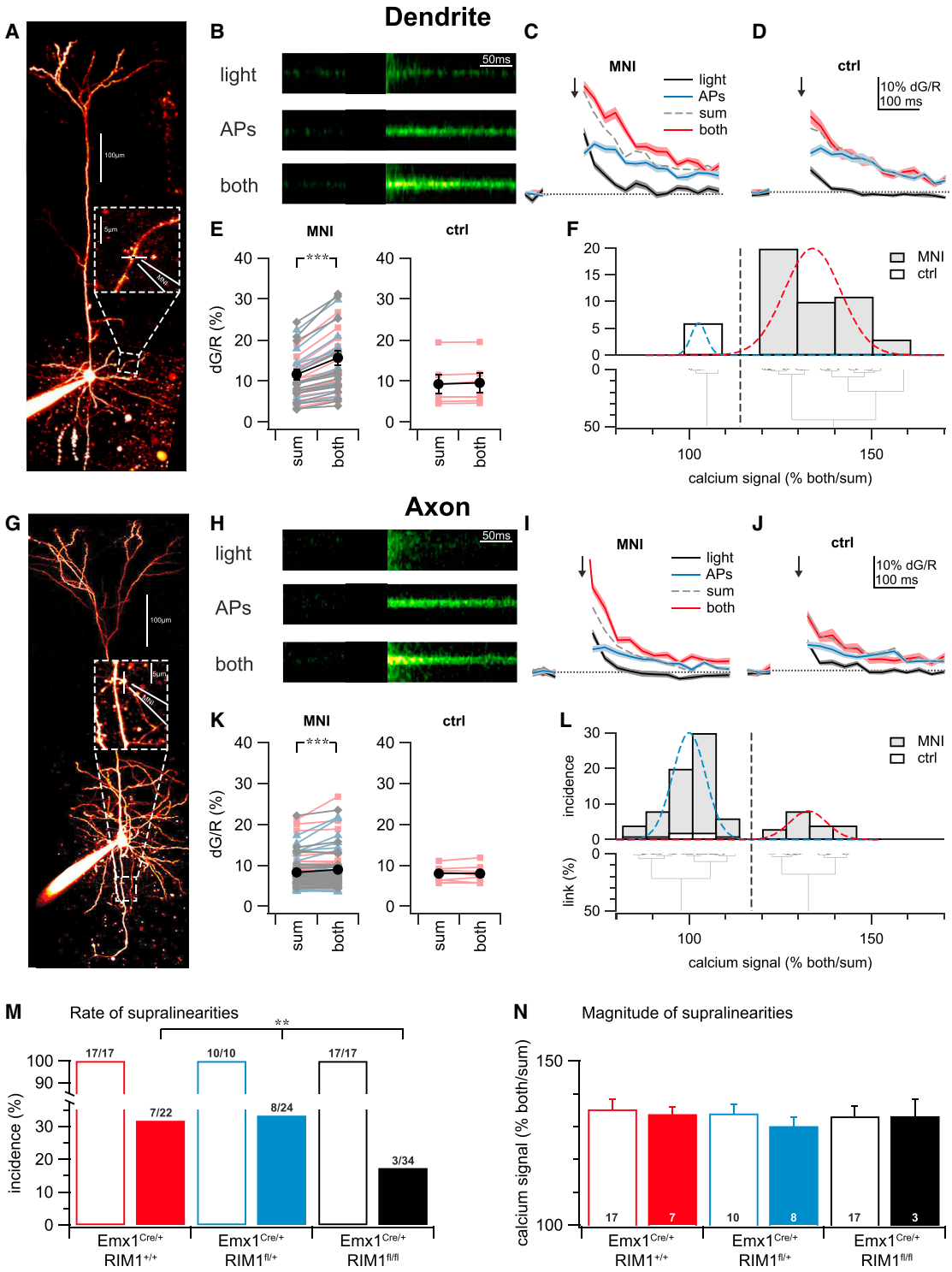

Figure 6. Incidence of Ca^{2+} Supralinearities Are Reduced in RIM1αβ KO Boutons

(A) 2PLSM maximum-intensity projection of PC filled with Alexa 594, indicating the dendritic location of line scan (white continuous line) and uncaging point (black break in white line). MNI-NMDA was locally puffed right next to uncaging point ("MNI").

(B) The three conditions "light" (2-ms-long uncaging pulse), "APs" (five APs at 50 Hz), and "both" (both simultaneously) were interleaved every 7 s and repeated nine times each (STAR Methods; Buchanan et al., 2012). Green intensity denotes the dG change in Fluo-5F signal averaged across the nine sweeps, then 2D median filtered with radius 1.5 pixels. To enable comparison, all three green color maps are set to the dynamic range of "both." Uncaging pulse artifact was blanked out.

(legend continued on next page)

with our previous study showing that preNMDARs are synapse-type-specifically expressed (Buchanan et al., 2012; Larsen and Sjöström, 2015).

We further analyzed both axonal and dendritic Ca^{2+} supralinearities to see if they varied with the three different genotypes, $Emx1^{Cre/+}$;$RIM1\alpha\beta^{+/+}$, $^{fl/+}$, and $^{fl/fl}$. Dendritic supralinearities were always found irrespective of whether RIM1αβ was knocked out or not (Figure 6M), consistent with RIMs being presynaptic, but not postsynaptic (Tang et al., 2016). Axonal supralinearities, however, decreased with RIM1αβ deletion (Figure 6M). The magnitude of supralinearities, however, was indistinguishable in dendrites as well as in axons of $Emx1^{Cre/+}$;$RIM1\alpha\beta^{+/+}$, $^{fl/+}$, and $^{fl/fl}$ mice (Figure 6N). The reduction of NMDA-evoked supralinearities in $Emx1^{Cre/+}$;$RIM1\alpha\beta^{fl/fl}$ mice suggested that preNMDARs depend on RIM1αβ for scaffolding (Figure S4). The ~90% efficacy of RIM1αβ deletion (Figure S5) could explain the 3 out of 34 remaining supralinear boutons in $Emx1^{Cre/+}$;$RIM1\alpha\beta^{fl/fl}$ mice (Figure 6M). In PC boutons of $Emx1^{Cre/+}$;$RIM1\alpha\beta^{fl/+}$ mice, however, even though preNMDAR regulation of RRP replenishment was completely abolished (Figure 4), Ca^{2+} supralinearities were still as prevalent as in $Emx1^{Cre/+}$;$RIM1\alpha\beta^{+/+}$ mice (Figure 6M). PreNMDARs may thus rely on RIM1αβ for both signaling and scaffolding.

To explore the impact of RIM1αβ KO on scaffolding of VDCCs, we analyzed AP-evoked Ca^{2+} transients in dendritic and axonal compartments (Figures S7A and S7B). AP-evoked Ca^{2+} signals in dendrites were unaffected by RIM1αβ KO but were gradually reduced in boutons (Figures S7C–S7F). These results reconfirmed RIM1 as an active-zone protein (Südhof, 2012) that tethers VDCCs (Han et al., 2011; Kaeser et al., 2011), but without any postsynaptic expression (Tang et al., 2016).

In summary, conditional RIM1αβ deletion reduced tethering of pre-, but not post-, synaptic NMDARs and VDCCs. These findings cement the already well-known role of RIM1 as a key presynaptic active-zone scaffolding protein. The presence of preNMDARs in heterozygous RIM1αβ mice furthermore suggests that these receptors also need RIM1 for signaling, directly or indirectly.

PreNMDAR Regulation of Spontaneous Release Is Intact in RIM1 KO Mice

To see whether preNMDAR-based regulation of spontaneous release also required RIM1, we carried out whole-cell recordings of spontaneous release onto L5 PCs and compared the impact of Ro in acute slices from $Emx1^{Cre/+}$;$RIM1\alpha\beta^{fl/fl}$ and $^{fl/+}$ mice with $Emx1^{Cre/+}$;$RIM1\alpha\beta^{+/+}$ littermates as well as with $RIM1\alpha\beta^{fl/fl}$;no-Cre controls. Recorded cells were clamped at −80 mV. In all four genotypes, Ro wash-in reduced mini frequency, but not amplitude (Figure 7), as in WT mice (Figure 2). Therefore, preNMDAR regulation of spontaneous release did not need RIM1.

Because competitive antagonists, such as AP5, and allosteric inhibitors, such as Ro, inhibit NMDARs by different mechanisms, we verified our negative result with Ro (Figure 7) using AP5. We found that AP5 reduced mini frequency, but not amplitude, in hetero- and homozygous RIM1αβ KOs as in littermate controls (Figure S8). PreNMDARs thus do not need RIM1αβ to regulate spontaneous release.

In RIM1αβ KO animals, baseline evoked release was reduced (Figure S6). Because evoked release (Figures 4 and 5), but not spontaneous release (Figure 7), depended on RIM1αβ, we speculated that baseline spontaneous release rates might be

(C) A supralinear Ca^{2+} response (red) was unsurprisingly obtained when combining uncaging (black) of MNI-NMDA ("MNI") and APs (blue; both 18% ± 0.8% versus APs/light sum 13% ± 2%, $p < 0.01$). The arithmetic sum of APs and uncaging is denoted by the gray dashed trace. Traces were smoothed in 30 ms time bins. Stimulation artifact was blanked. Arrow indicates start of both 50 Hz AP train and uncaging pulse. Traces show dG/R mean ± SEM.
(D) In the absence of MNI-NMDA ("ctrl"), Ca^{2+} supralinearities were eliminated (both 12% ± 0.6% versus sum 12% ± 0.6%, $p = 0.765$).
(E) Dendritic Ca^{2+} supralinearities were consistently elicited in the presence of MNI-NMDA (left, "MNI"). Data were pooled from $Emx1^{Cre/+}$;$RIM1\alpha\beta^{+/+}$ (red squares), $Emx1^{Cre/+}$;$RIM1\alpha\beta^{fl/+}$ (blue triangles), and $Emx1^{Cre/+}$;$RIM1\alpha\beta^{fl/fl}$ (gray diamonds) mice, as they were indistinguishable ($p_{ANOVA} = 0.87$ for both/sum, n = 17, 10, 17; see M and N for additional statistics). $Emx1^{Cre/+}$;$RIM1\alpha\beta^{+/+}$ controls showed no supralinearities in the absence of MNI-NMDA (right, "ctrl").
(F) Based on the normalized Ca^{2+} transients (both/sum), hierarchical agglomerative clustering autonomously categorized control ("ctrl") and uncaging experiments ("MNI") into distinct classes. The vertical dashed line indicates the demarcation boundary between classes. Gaussians show class mean and standard deviation.
(G) An axon collateral splitting off the main axon (asterisk) is branching into the basal dendritic arbour (arrowheads). Inset: line scan location (white line), uncaging point (black dot), and MNI-NMDA puffing pipette, as in (A).
(H) "Light," "APs," and "both" denote interleaved averages of nine line scans, with the artifact blanked out (as in A).
(I) During MNI-NMDA puff ("MNI"), a supralinear response (red) was obtained in this bouton (G and H) during coincident uncaging (black) and APs (blue; both 11% ± 0.5% versus sum 7.3% ± 0.7%, $p < 0.01$).
(J) No such bouton supralinearity was obtained in the absence of MNI-NMDA (both 7.5% ± 0.8% versus sum 8.6% ± 0.8%, $p = 0.338$).
(K) In the presence of MNI-NMDA (left, "MNI"), axonal boutons had supralinearities. Data were pooled from $Emx1^{Cre/+}$;$RIM1\alpha\beta^{+/+}$ (red squares), $Emx1^{Cre/+}$;$RIM1\alpha\beta^{fl/+}$ (blue triangles), or $Emx1^{Cre/+}$;$RIM1\alpha\beta^{fl/fl}$ (gray diamonds) mice, as they were indistinguishable ($p_{ANOVA} = 0.17$ for both/sum, n = 22, 24, 34; see M and N for additional statistics). In the absence of MNI-NMDA (right, "ctrl"), no supralinearities were found in $Emx1^{Cre/+}$;$RIM1\alpha\beta^{+/+}$ controls.
(L) Clustering independently classified axonal boutons into two types: one with supralinearities (such as example in G–J; 22 of 63 boutons across all genotypes) and the other with controls. Vertical dashed line denotes demarcation boundary. Gaussians show class mean and standard deviation.
(M) Incidence of axonal bouton supralinearities decreased with RIM1αβ KO (solid bars; Cochran-Armitage test for trend: $p < 0.01$; three-way chi-square: $p < 0.05$). Dendritic supralinearities, however, were unaffected (open bars). Numbers above bars indicate supralinear out of total number of line scans—7 of 22 supralinear boutons for $Emx1^{Cre/+}$;$RIM1\alpha\beta^{+/+}$ were indistinguishable from 12 of 22 in Buchanan et al. (2012) ($p = 0.128$, chi-square test). The number of cells were n = 6, 5, and 7 for $Emx1^{Cre/+}$;$RIM1\alpha\beta^{+/+}$, $Emx1^{Cre/+}$;$RIM1\alpha\beta^{fl/+}$, and $Emx1^{Cre/+}$;$RIM1\alpha\beta^{fl/fl}$, respectively.
(N) The magnitude of bouton supralinearities was not affected by KO of RIM1αβ (Kendall tau test; $p = 0.544$; t test for Pearson's r gave $p = 0.693$ for $r = -0.1$; ANOVA $p = 0.613$). The magnitude of dendritic supralinearities also showed no distinguishable trend (Kendall's tau test: $p = 0.420$; t test for Person's r: $p = 0.596$, $r = -0.082$; ANOVA $p = 0.869$). Hierarchical clustering was used to select supralinear responses (to the right of vertical dashed demarcation line in F and L). See also Figure S7.

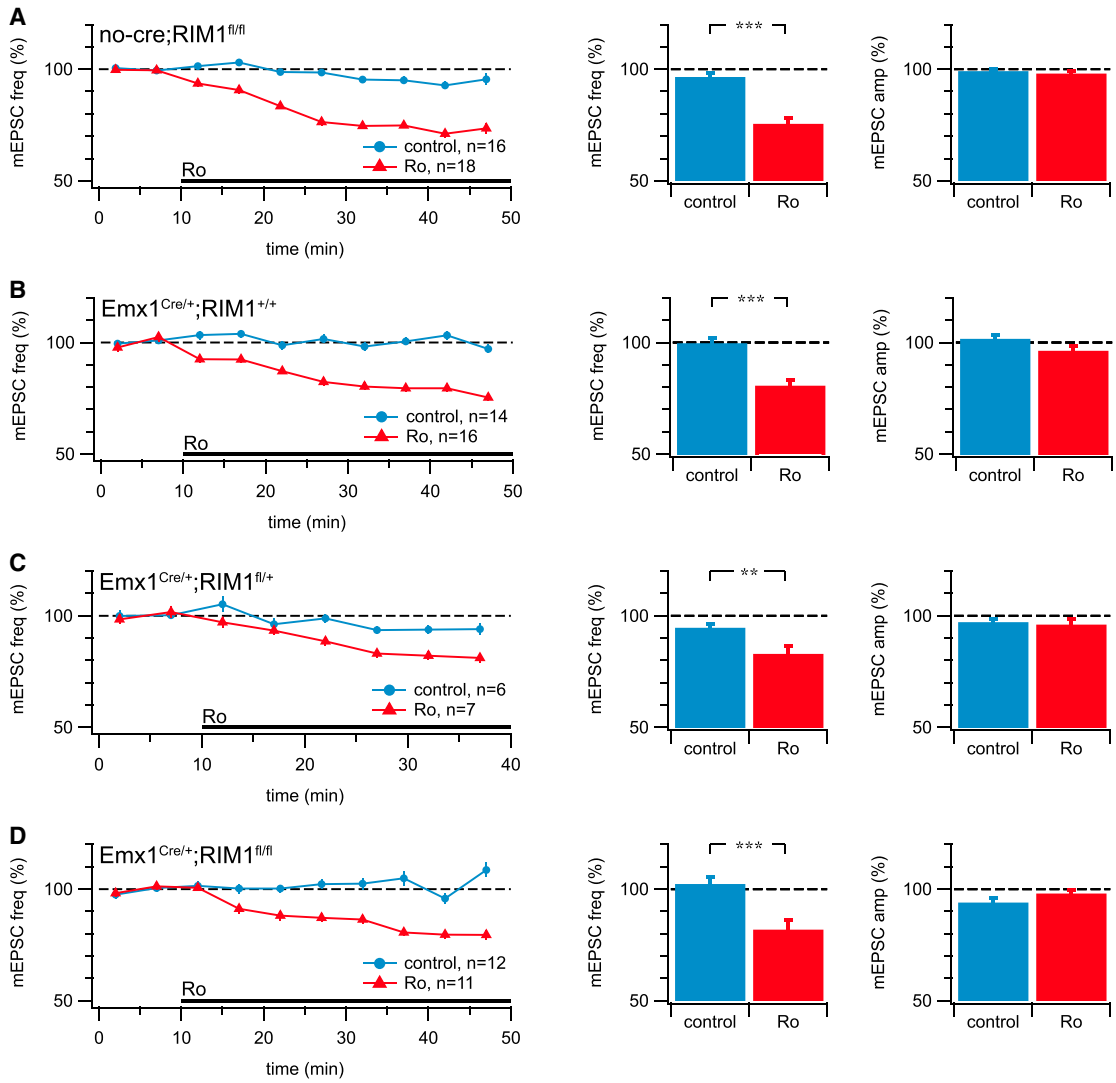

Figure 7. PreNMDAR-Dependent Regulation of Spontaneous Release Is Unaffected by RIM1αβ Knockout

Ro wash-in reduced mini frequency, but not amplitude, in RIM1αβ$^{fl/fl}$;no-Cre (A, red) and in Emx1$^{Cre/+}$;RIM1αβ$^{+/+}$ L5 PCs (B, red), as expected from previous results (Figure 2) (Berretta and Jones, 1996; Sjöström et al., 2003). In heterozygous Emx1$^{Cre/+}$;RIM1αβ$^{fl/+}$ (C, red) or homozygous Emx1$^{Cre/+}$;RIM1αβ$^{fl/fl}$ (D, red) KO PCs, the results were indistinguishable, showing that preNMDAR-mediated regulation of spontaneous release did not rely directly on RIM1 (also see Figure S8). Blue denotes mock wash-in controls (A–D). Experimental details as in Figure 2 (STAR Methods).
See also Figures S8 and S9 and Tables S1 and S2.

unaffected in RIM1αβ KO mice. Surprisingly, both mini frequency and amplitude were elevated in Emx1$^{Cre/+}$;RIM1αβ$^{fl/fl}$ animals, but not in Emx1$^{Cre/+}$;RIM1αβ$^{+/+}$ or $^{fl/+}$ littermates (Figure S9).

An increase in mini frequency could be attributed to an increase in the rate of spontaneous release or to an increased synaptic density, which might be reflected in connectivity rates. To investigate whether PC-PC connectivity was increased in RIM1αβ$^{-/-}$ animals, we retrospectively analyzed the likelihood of finding monosynaptic connections in 3,491 whole-cell recordings across different RIM1 genotypes (e.g., data in Figures 4 and 5; Figure S6). We did not, however, find any differences in connectivity (Table S1). We verified these findings by counting postsynaptic spines in L5 PC basal dendritic arbors (where L5 PCs receive most synapses from other L5 PCs, see Markram et al., 1997) and again found no differences in spine density (Table S2).

We conclude that preNMDAR-mediated upregulation of spontaneous release did not rely on RIM1αβ. In addition, homozygous RIM1αβ KO boosted baseline rate and amplitude of spontaneous release, further strengthening the general finding that evoked and spontaneous release are regulated separately (Figures S6 and S7).

Regulation of Spontaneous Release by PreNMDARs Requires JNK2

In layer II PCs of mouse entorhinal cortex, preNMDARs rely on JNK2 to upregulate spontaneous release (Nisticò et al., 2015).

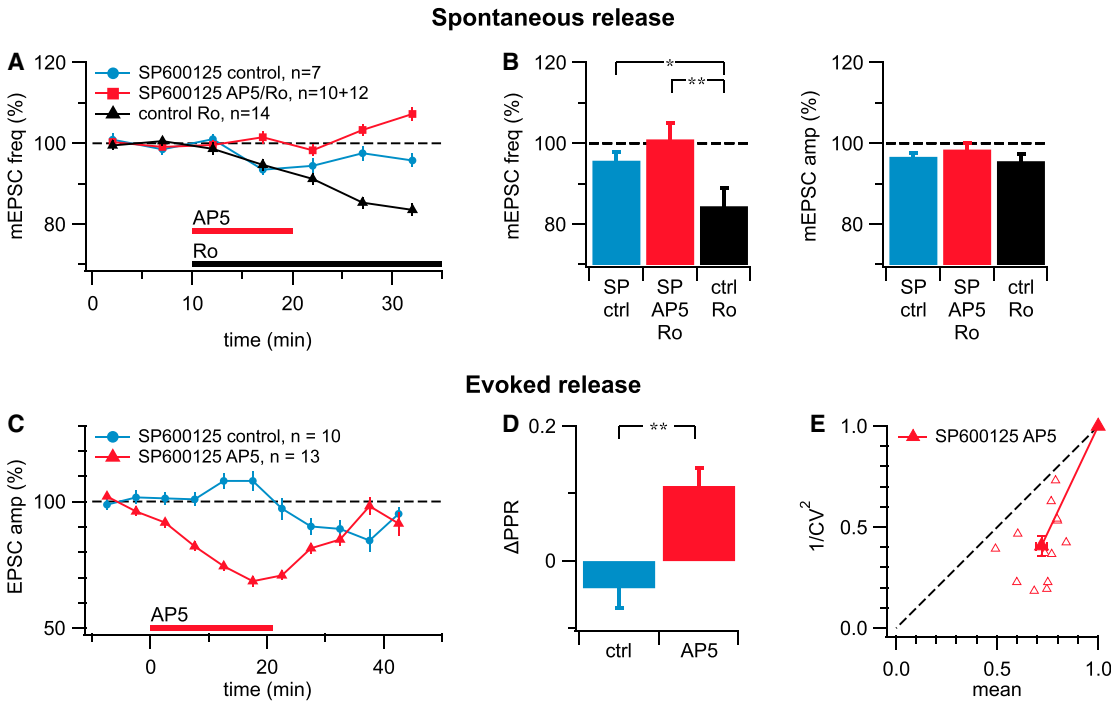

Figure 8. PreNMDAR-Dependent Regulation of Spontaneous, but Not Evoked, Release Depends on JNK2 Signaling

(A) Ro reliably reduced mini frequency in interleaved positive controls (black triangles), but AP5 or Ro wash-in after JNK2 blockade with SP600125 ("SP," red squares) was ineffectual. AP5 and Ro were pooled as they were indistinguishable (94% ± 6%, n = 10 versus 110% ± 5%, n = 12, p = 0.086). SP-only mock wash-in control experiments were stable (blue circles). SP was present for 2 hr before, as well as during, the experiment (STAR Methods).

(B) Ro wash-in consistently reduced mini frequency, but not amplitude, in positive controls ("ctrl Ro"), consistent with a presynaptic locus. However, Ro or AP5 wash-in after JNK2 blockade with SP ("SP AP5 Ro") was indistinguishable from SP-only negative controls ("SP ctrl"), demonstrating that in visual cortex L5 PCs, preNMDARs relied on JNK2 signaling to regulate spontaneous release, as previously shown in entorhinal cortex (Nisticò et al., 2015).

(C) In the presence of SP, preNMDAR blockade still reduced evoked release (red triangles; 72% ± 3%, n = 13, p < 0.001 versus 100%), while SP-only controls remained stable (blue circles; 100% ± 5%, n = 10; p = 0.371 versus 100%; p < 0.001 versus red), showing that preNMDAR-dependent regulation of evoked release did not require intact JNK2 signaling.

(D) Whereas control PPR remained unaffected in SP, AP5 increased PPR, in agreement with our previous data indicating a presynaptic locus (e.g., Figure 1).

(E) AP5 altered CV in agreement with a reduction of p_r (19° ± 2°, n = 13, p < 0.001), whereas no effect was found in controls (−10° ± 20°, n = 10, p = 0.663).

To see whether this was also true for visual cortex L5 PCs, we incubated acute slices with the JNK2-specific inhibitor SP600125 (SP; see STAR Methods; Bennett et al., 2001). Cells were voltage clamped at −80 mV. In SP, neither Ro nor AP5 wash-in affected spontaneous release (Figures 8A–8C), suggesting that preNMDAR regulation of mini frequency relied on JNK2. Interleaved controls with Ro wash-in reliably reduced mini frequency, but not amplitude, and mock wash-in controls revealed that SP itself had no short-term effects (Figures 8A–8C). JNK2 signaling did not depend on RIM1, as SP was still effective in $Emx1^{Cre/+}$;$RIM1\alpha\beta^{fl/fl}$ mice (mini frequency after/before Ro: 105% ± 10%, n = 6, p = 0.68, one-sample t test; amplitude after/before Ro: 105% ± 4%, p = 0.34, one-sample t test; data not shown).

Although the specificity of SP for JNK2 was previously demonstrated in JNK2 KO animals (Nisticò et al., 2015), we verified the SP results with another JNK blocker, TCS JNK 6o (TCS) (Szczepankiewicz et al., 2006), at a concentration that blocks JNK1-3 (STAR Methods). In TCS, Ro wash-in had no effect on mini frequency (after/before TCS control: 104% ± 10%, n = 3 versus TCS+Ro: 101% ± 6%, n = 6, p = 0.81) or amplitude (TCS control: 101% ± 1%, n = 3 versus TCS+Ro: 98% ± 2%, n = 6, p = 0.29; data not shown), confirming the SP results.

We wondered whether JNK blockade resulted in occlusion, in which case SP and TCS should reduce baseline mini frequency. We found, however, that both SP and TCS boosted baseline spontaneous release rates (SP: 4 ± 0.2 Hz, n = 43 or TCS: 4.5 ± 0.7 Hz, n = 18 versus WT controls: 2.6 ± 0.12 Hz, n = 123, p < 0.001 and p < 0.05, respectively, p_{ANOVA} < 0.001, data not shown) without affecting mini amplitude (SP: −12 ± 0.2 pA or TCS: −11 ± 0.5 pA versus WT controls: −12 ± 0.2 pA, p = 0.093 and p = 0.52, respectively, p_{ANOVA} = 0.216, data not shown). These results argue against occlusion and in favor of signaling blockade.

We explored whether JNK2 blockade affected preNMDAR regulation of evoked release. We found that SP had no impact on the suppression of evoked release by AP5 (Figures 8C–8E). EPSCs were recorded at −80 mV to block postsynaptic NMDARs. SP-only controls verified that JNK2 blockade did not affect evoked release (Figures 8C–8E).

PreNMDARs thus need JNK to regulate spontaneous, but not evoked, release (Figure 8). This echoes the need for RIM1αβ in

preNMDAR regulation of evoked, but not spontaneous, release (Figures 4 and 5 versus Figure 7), thus revealing a double dissociation.

DISCUSSION

Here, we provide several lines of evidence that preNMDARs signal differentially to control evoked and spontaneous release by independent and non-overlapping mechanisms. First, preNMDARs upregulate RRP replenishment rates to indirectly sustain p_r during high-frequency firing. Second, at low frequencies, preNMDARs regulate spontaneous, but not evoked, release. Third, evoked, but not spontaneous, release is sensitive to Mg^{2+}. Fourth, preNMDAR regulation of evoked release—but not of spontaneous release—is abolished when RIM1$\alpha\beta$ is conditionally knocked out. Fifth, like in entorhinal cortex (Nisticò et al., 2015), preNMDAR regulation of spontaneous release is abolished by JNK2 blockade, but we additionally demonstrate that evoked release is not.

PreNMDARs and Evoked Release

PreNMDARs in L5 PCs have a dual role, controlling both short-term and long-term plasticity (Sjöström et al., 2003). Here, we focused on the role of preNMDARs in short-term plasticity. We have shown before, using internal loading of the channel-pore blocker MK-801, that the NMDARs that control evoked release are in the presynaptic, but not the postsynaptic, cell, and we also demonstrated the existence of NMDA-evoked axonal supralinearities (Buchanan et al., 2012), which we reproduced here. By depleting monosynaptic PC-PC connections, we found here that preNMDAR blockade downregulated both RRP size and replenishment rate. This contrasted with reduced Ca^{2+}, which only affected the RRP size, as previously shown at the Calyx of Held (Schneggenburger et al., 1999). As the SMN method suffers from certain pitfalls (Kaeser and Regehr, 2017; Neher, 2015), we fit the TM short-term plasticity model as an alternative and obtained the equivalent results. It is not clear, however, that either the SMN or the TM methods necessarily reflect solely a change in RRP size or a change in p_r (Kaeser and Regehr, 2017; Neher, 2015). For example, a perceived decrease in RRP size might also reflect a less complete depletion of the RRP after lowering p_r. For our study, this caveat matters little, as the key difference was that preNMDAR blockade altered RRP recovery kinetics whereas Ca^{2+} reduction did not. In other words, preNMDAR action extended beyond that of fluxing Ca^{2+}. As has been shown for postsynaptic NMDARs, preNMDARs may signal metabotropically, form Ca^{2+} nanodomains, or both. However, our previous work showed that both external and internal MK-801 downregulate evoked release (Buchanan et al., 2012; Sjöström et al., 2003), which argues against metabotropic NMDAR signaling in the regulation of evoked release (Nabavi et al., 2013).

As a most parsimonious interpretation, we propose that preNMDARs act directly on the RRP replenishment rate, whereas the effects on the RRP size and p_r are secondary. One caveat is that we cannot distinguish replenishment from recycling. Another caveat is that preNMDARs may act via presynaptic VDCCs to control replenishment, since RIM1 KO also reduced VDCC-mediated signals (Figure S7). Similarly, we cannot exclude direct regulatory action of preNMDARs on RRP size, vesicular p_{ves}, and/or synaptic p_r in addition to that on replenishment rate. However, the indirect action of preNMDARs on p_r via the RRP replenishment rate is intuitively appealing since it helps explain why preNMDAR blockade requires more time to express than Ca^{2+} reduction does (Figure 3). One testable prediction of our interpretation is that even at high frequencies, no effects of preNMDAR blockade may be discernible unless the RRP is depleted with a sufficient number of APs.

Because GluN2B-containing NMDARs are blocked by Mg^{2+} (Paoletti et al., 2013), NMDA autoreceptors in L5 PC axons should be preferentially activated by presynaptic spiking above the critical frequency, which we measured to ~8 Hz, when the dual need for depolarization and glutamate is satisfied. PreNMDARs may thus act as detectors of presynaptic high-frequency activity. In agreement, preNMDAR blockade had no effect when presynaptic high-frequency firing was temporarily paused. Interestingly, this high-pass filtering is found for short-term, but not long-term, plasticity in L5 PCs (Sjöström et al., 2003), although long-term plasticity in the cerebellum is also high-pass filtered by preNMDARs (Bidoret et al., 2009) and preNMDARs in hippocampus band-pass filter at theta frequency (McGuinness et al., 2010). At L5 PC-PC connections, preNMDARs may thus serve to upregulate vesicle replenishment rates during periods of elevated activity.

PreNMDARs and Spontaneous Release

It has been long known that preNMDAR blockade downregulates spontaneous release (Berretta and Jones, 1996; Sjöström et al., 2003). What has been unclear, however, is how pharmacological blockade of presumably already Mg^{2+}-blocked preNMDARs could possibly downregulate spontaneous release. Several solutions to this conundrum have been proposed, one of which is that preNMDARs are not actually blocked by Mg^{2+}. At this developmental stage, preNMDARs at inputs to L2/3 PC of the mouse visual cortex contain the GluN3A subunit, which confers Mg^{2+} insensitivity (Larsen et al., 2011). This allows them to be tonically active during mini recordings: in GluN3A null mice, there is no effect from AP5 application on mini frequency in L2/3 PCs unless the Mg^{2+} concentration is lowered (Larsen et al., 2011). For L2/3 PCs, the GluN3A subunit may thus be critical for preNMDARs to influence spontaneous release—it would be interesting to know whether this is the case in L5 PCs as well. Furthermore, there is evidence showing that preNMDAR regulation of spontaneous release onto mouse visual cortex L2/3 PCs does not depend on Ca^{2+} (Kunz et al., 2013). The relevance of Mg^{2+} blockade for preNMDAR-mediated regulation of spontaneous release is therefore unclear. One possibility for L5 PCs is that preNMDARs regulate evoked and spontaneous release via different signaling modes, e.g., one metabotropically and the other ionotropically. Another possibility is that the NMDARs that regulate spontaneous release are elsewhere. However, it is not likely that postsynaptic NMDARs regulate spontaneous release, since those were not sensitive to Ro (Figures S1 and S2) (Sjöström et al., 2003; Stocca and Vicini, 1998), whereas mini frequency was (Figures 2, 7, and 8) (Sjöström et al., 2003). The details of the downstream signaling is largely unknown,

although preNMDAR regulation of spontaneous release in L2/3 PCs relies on PKC (Kunz et al., 2013).

RIMs and the Regulation of Neurotransmitter Release

PreNMDAR regulation of evoked release required RIM1αβ, since it was abolished in heterozygous RIM1αβ KO mice, but precisely how preNMDARs signal to control evoked release remain unclear. It is known that protein kinase A (PKA) and RIM are in the same pathway (Castillo et al., 2002), and PKA modifies RIM1α in lateral amygdala long-term plasticity (Fourcaudot et al., 2008). It is therefore tempting to speculate that PKA acts downstream of preNMDARs to control evoked release at L5 PC synapses. However, phosphorylation of RIM1α is not necessary for PKA-dependent long-term plasticity *in vivo* (Kaeser et al., 2008a), suggesting a more complex functional relationship between PKA and RIM1.

The abolishment of preNMDAR control of release in heterozygous animals was unexpected and suggested haploinsufficiency. Although germline recombination would be an alternative interpretation, several lines of evidence argue against this view. First, RIM1αβ null mouse survival rates are poor (Kaeser et al., 2008b). Second, the genotyping primers were designed to fail to amplify in null animals. Third, reporter line crosses (Figure S5) did not indicate germline recombination. To better understand this RIM1αβ haploinsufficiency, we looked for preNMDAR Ca^{2+} supralinearities in RIM1αβ deletion mice. As RIMs have a dual role in scaffolding and in signaling (Südhof, 2012), we argued that there were two possible outcomes. If preNMDARs need RIM1 for scaffolding, then preNMDAR Ca^{2+} supralinearities should be abolished in RIM1αβ deletion mice. But if preNMDARs rely on RIM1 for signaling, then bouton supralinearities should still be present in RIM1αβ deletion mice. As expected, we saw a reduction in AP-mediated Ca^{2+} signals in RIM1αβ KO mice, consistent with reduced tethering and increased fluidity of active-zone VDCCs (Han et al., 2011; Kaeser et al., 2011). Additionally, we found that the incidence of NMDA-triggered Ca^{2+} supralinearities in axonal boutons were reduced in RIM1αβ deletion mice, suggesting that RIM1 provides scaffolding for these preNMDARs. The co-immunoprecipitation of GluN2B and RIM1αβ was consistent with such an association, although it need not be direct. However, the presence of preNMDAR supralinearities in $Emx1^{Cre/+}$; $RIM1\alpha\beta^{fl/+}$ PC axons suggested that the complete abolishment of preNMDAR regulation of evoked release in L5 PC-PC pairs of heterozygotes was due to a need for RIM1αβ in signaling rather than in scaffolding. PreNMDARs may thus rely on RIM1αβ for both scaffolding and for signaling. Another not mutually exclusive possibility is that in regulating evoked release, preNMDARs rely on a subset of presynaptic VDCCs tethered by RIM1αβ so that the need for RIM1αβ is indirect. Indeed, we found evidence that p_r was reduced at L5 PC-PC connections in RIM1αβ deletion mice: responses were smaller and PPR increased. This finding is consistent with prior studies, e.g., in the Calyx of Held and in the hippocampal CA1 region, showing that p_r is reduced in RIM1αβ KO mice (Han et al., 2011; Kaeser et al., 2008b, 2011; Schoch et al., 2002). RIM1αβ deletion may thus have occluded the effects of preNMDAR blockade.

To regulate spontaneous release, preNMDARs did not need RIM1αβ. We therefore expected baseline mini frequency and amplitude to be unaffected in RIM1αβ KO animals. To our surprise, we found that both mini frequency and amplitude were increased in homozygous, but not heterozygous, RIM1αβ deletion mice. We could not attribute this to increased synapse density. This upregulation in RIM1αβ KO animals might be a form of homeostatic plasticity to compensate for the reduced evoked release (Maheux et al., 2015). Regardless, our findings support the view that evoked and spontaneous release are separately regulated processes (Kavalali, 2015).

A Double Dissociation of Presynaptic NMDA Receptor Signaling

A long-standing question in the field is what permits preNMDARs to regulate low-frequency spontaneous release while selectively influencing only high-frequency evoked release (Banerjee et al., 2016). It has long been speculated that the mechanisms for preNMDAR-mediated regulation of evoked and spontaneous release must be different (Brasier and Feldman, 2008; Sjöström et al., 2003). Here, we report that preNMDARs rely on RIM1αβ to regulate evoked, but not spontaneous, release and, conversely, that they require JNK2 to control spontaneous, but not evoked, release, thus revealing a double dissociation. Although the details of the individual signaling cascades remain to be teased apart, this double dissociation offers a plausible answer to this long-standing question, as preNMDAR regulation of evoked and spontaneous release appear to be entirely separate. Additionally, based on differential Mg^{2+} dependence, the former may be ionotropic while the latter may be metabotropic (Nabavi et al., 2013). This dissociation of preNMDAR signaling supports the emerging evidence that spontaneous and evoked transmission function via different mechanisms, possibly acting on different pools of vesicles (Kavalali, 2015) that may be physically separated by RIM nanocolumns (Tang et al., 2016) or that are not even located at the same synapses (Melom et al., 2013; Reese and Kavalali, 2016). Another possibility is that these vesicle pools are the same but that, e.g., the Ca^{2+} sensors for evoked and spontaneous release are distinct (Groffen et al., 2010). Either way, this careful regulation of spontaneous release supports the view that minis are not noise but functionally important, e.g., for homeostatic plasticity, for synaptic maturation, and in neuropsychiatric pathology (Kavalali, 2015).

Although evoked release in our study originates from L5 PCs, we cannot draw strong conclusions about the origin of spontaneous release. Irrespective of their location, however, preNMDAR signaling controlling evoked and spontaneous release would be doubly dissociated. In fact, this double dissociation suggests that these two forms of regulation need not co-exist. Indeed, entorhinal cortex preNMDARs regulate spontaneous release (Berretta and Jones, 1996; Nisticò et al., 2015), but no effect on evoked release has been found (Sparks and Chapman, 2014).

Outlook

PreNMDARs have been surrounded by debate, mostly regarding their function and precise location (Banerjee et al., 2016; Duguid and Sjöström, 2006). Much disagreement has centered on their location, with some studies failing to find evidence for axonal NMDARs (e.g., Christie and Jahr, 2009).

We reproduce here our finding that preNMDAR supralinearities are only found at a subset of boutons (Buchanan et al., 2012), which helps explain such disagreements. Furthermore, by dissociating preNMDAR signaling in evoked and spontaneous release, our study provides resolution to the long-standing conundrum of how these can be differentially regulated (Banerjee et al., 2016).

NMDAR dysfunction has been implicated in neurological disorders such as pathological pain, schizophrenia, stroke, and neurodegenerative disease (Paoletti et al., 2013). This has resulted in an increasing interest in new drugs targeting NMDARs, which requires an improved understanding of unconventional NMDAR signaling modes, e.g., without Ca^{2+} (Nabavi et al., 2013) or presynaptically (Banerjee et al., 2016). Though a specific role for preNMDARs in disease has been relatively overlooked, preNMDARs have been implicated in epilepsy, cortical rewiring following lesion, and dyslexia (Banerjee et al., 2016). Elucidating the signaling downstream of preNMDARs is thus a crucial step toward an improved understanding of the roles these receptors play in health and disease. The present study lays a foundation for future work on preNMDAR signaling mechanisms.

STAR★METHODS

Detailed methods are provided in the online version of this paper and include the following:

- KEY RESOURCES TABLE
- CONTACT FOR REAGENT AND RESOURCE SHARING
- EXPERIMENTAL MODEL AND SUBJECT DETAILS
- METHOD DETAILS
  - Slice Preparation and Basic Electrophysiology
  - Evoked Release
  - Spontaneous Release
  - Pharmacology
  - 2PLSM and Uncaging
  - Computer Modeling
  - Western Blotting
  - Co-immunoprecipitation
- QUANTIFICATION AND STATISTICAL ANALYSIS

SUPPLEMENTAL INFORMATION

Supplemental Information includes nine figures and two tables and can be found with this article online at https://doi.org/10.1016/j.neuron.2017.09.030.

A video abstract is available at https://doi.org/10.1016/j.neuron.2017.09.030#mmc3.

AUTHOR CONTRIBUTIONS

T.A., S.Y.L., J.A.B., K.A.B., D.E., A.V.B., R.P.C., J.O., and P.J.S. carried out the evoked release experiments. A.M., S.Y.L., C.Y.C.C., A.T.-J., J.A.B., and K.A.B. undertook the spontaneous release experiments. C.Y.C.C. carried out uncaging, Ca^{2+}, and spine imaging experiments. J.A.B. carried out spine counts on C.Y.C.C.'s data and connectivity analysis on T.A.'s data. R.P.C. carried out computer simulations. Transgenic crosses and genotyping were designed by W.T.F. and K.K.M. and carried out by E.N., T.A., S.Y.L., C.Y.C.C., and J.A.B. E.N. carried out the western blots and the co-immunoprecipitation, with guidance from W.T.F. and K.K.M. All team members analyzed their own data. P.J.S. conceived of the project together with co-authors and wrote all in-house software. P.J.S. and co-authors wrote the manuscript.

ACKNOWLEDGMENTS

We thank Alanna Watt, Mark van Rossum, Charles Bourque, Andrew Chapman, Wade Regehr, Yuki Goda, Rylan Larsen, Guy Bouvier, Ed Ruthazer, Tiago Branco, Ian Duguid, Thomas Nevian, Zoltan Nusser, Sabrina Chierzi, Emma Jones, and Sjöström lab members for help and useful discussions. We thank the RI MUHC Molecular Imaging Platform for support and Pascal Kaeser for the kind gift of the RIM1$\alpha\beta^{fl/fl}$ mice.

This work was funded by CFI LOF 28331 (P.J.S.), CIHR OG 126137 (P.J.S.), CIHR NIA 288936 (P.J.S.), NSERC DG 418546-2 (P.J.S.), NSERC DG 2017-04730 (P.J.S.), NSERC DAS 2017-507818 (P.J.S.), CIHR OG PJT148569 (K.K.M.), NSERC DG 69404 (K.K.M.), Brain Canada/W. Garfield Weston Foundation (K.K.M.), MRC CDA G0700188 (P.J.S.), EU FP7 FET-Open grant 243914 (P.J.S.), the Max Stern Award (J.A.B.), BBSRC Industrial CASE Award BB/H016600/1 (A.V.B.), UCL Impact Studentship (J.O.), UCL Neuroscience MSc program (A.A.T.-J.), Royal Society Industry Fellowship IF080019/AM (D.E.), EPSRC EP/F500385/1 (R.P.C.), BBSRC BB/F529254/1 (R.P.C.), Fundação para a Ciência e a Tecnologia SFRH/BD/60301/2009 (R.P.C.), and an RI MUHC postdoctoral fellowship (W.T.F.).

Received: April 24, 2017
Revised: August 3, 2017
Accepted: September 19, 2017
Published: October 12, 2017

REFERENCES

Abrahamsson, T., Lalanne, T., Watt, A.J., and Sjöström, P.J. (2016). In vitro investigation of synaptic plasticity. Cold Spring Harb. Protoc. Published online June 1, 2016. https://doi.org/10.1101/pdb.top087262.

Banerjee, A., Larsen, R.S., Philpot, B.D., and Paulsen, O. (2016). Roles of presynaptic NMDA receptors in neurotransmission and plasticity. Trends Neurosci. *39*, 26–39.

Bennett, B.L., Sasaki, D.T., Murray, B.W., O'Leary, E.C., Sakata, S.T., Xu, W., Leisten, J.C., Motiwala, A., Pierce, S., Satoh, Y., et al. (2001). SP600125, an anthrapyrazolone inhibitor of Jun N-terminal kinase. Proc. Natl. Acad. Sci. USA *98*, 13681–13686.

Berretta, N., and Jones, R.S. (1996). Tonic facilitation of glutamate release by presynaptic N-methyl-D-aspartate autoreceptors in the entorhinal cortex. Neuroscience *75*, 339–344.

Bidoret, C., Ayon, A., Barbour, B., and Casado, M. (2009). Presynaptic NR2A-containing NMDA receptors implement a high-pass filter synaptic plasticity rule. Proc. Natl. Acad. Sci. USA *106*, 14126–14131.

Blackman, A.V., Abrahamsson, T., Costa, R.P., Lalanne, T., and Sjöström, P.J. (2013). Target cell-specific short-term plasticity in local circuits. Front. Synaptic Neurosci. Published online December 6, 2013. https://doi.org/10.3389/fnsyn.2013.00011.

Brasier, D.J., and Feldman, D.E. (2008). Synapse-specific expression of functional presynaptic NMDA receptors in rat somatosensory cortex. J. Neurosci. *28*, 2199–2211.

Buchanan, K.A., Blackman, A.V., Moreau, A.W., Elgar, D., Costa, R.P., Lalanne, T., Tudor Jones, A.A., Oyrer, J., and Sjöström, P.J. (2012). Target-specific expression of presynaptic NMDA receptors in neocortical microcircuits. Neuron *75*, 451–466.

Castillo, P.E., Schoch, S., Schmitz, F., Südhof, T.C., and Malenka, R.C. (2002). RIM1alpha is required for presynaptic long-term potentiation. Nature *415*, 327–330.

Chevaleyre, V., Heifets, B.D., Kaeser, P.S., Südhof, T.C., and Castillo, P.E. (2007). Endocannabinoid-mediated long-term plasticity requires cAMP/PKA signaling and RIM1alpha. Neuron *54*, 801–812.

Christie, J.M., and Jahr, C.E. (2009). Selective expression of ligand-gated ion channels in L5 pyramidal cell axons. J. Neurosci. *29*, 11441–11450.

Costa, R.P., Sjöström, P.J., and van Rossum, M.C.W. (2013). Probabilistic inference of short-term synaptic plasticity in neocortical microcircuits. Front. Comput. Neurosci. *7*, 75.

Duguid, I., and Sjöström, P.J. (2006). Novel presynaptic mechanisms for coincidence detection in synaptic plasticity. Curr. Opin. Neurobiol. *16*, 312–322.

Fourcaudot, E., Gambino, F., Humeau, Y., Casassus, G., Shaban, H., Poulain, B., and Lüthi, A. (2008). cAMP/PKA signaling and RIM1alpha mediate presynaptic LTP in the lateral amygdala. Proc. Natl. Acad. Sci. USA *105*, 15130–15135.

Gorski, J.A., Talley, T., Qiu, M., Puelles, L., Rubenstein, J.L., and Jones, K.R. (2002). Cortical excitatory neurons and glia, but not GABAergic neurons, are produced in the Emx1-expressing lineage. J. Neurosci. *22*, 6309–6314.

Groffen, A.J., Martens, S., Díez Arazola, R., Cornelisse, L.N., Lozovaya, N., de Jong, A.P., Goriounova, N.A., Habets, R.L., Takai, Y., Borst, J.G., et al. (2010). Doc2b is a high-affinity Ca2+ sensor for spontaneous neurotransmitter release. Science *327*, 1614–1618.

Han, Y., Kaeser, P.S., Südhof, T.C., and Schneggenburger, R. (2011). RIM determines Ca^{2+} channel density and vesicle docking at the presynaptic active zone. Neuron *69*, 304–316.

Kaeser, P.S., and Regehr, W.G. (2017). The readily releasable pool of synaptic vesicles. Curr. Opin. Neurobiol. *43*, 63–70.

Kaeser, P.S., Kwon, H.B., Blundell, J., Chevaleyre, V., Morishita, W., Malenka, R.C., Powell, C.M., Castillo, P.E., and Südhof, T.C. (2008a). RIM1alpha phosphorylation at serine-413 by protein kinase A is not required for presynaptic long-term plasticity or learning. Proc. Natl. Acad. Sci. USA *105*, 14680–14685.

Kaeser, P.S., Kwon, H.B., Chiu, C.Q., Deng, L., Castillo, P.E., and Südhof, T.C. (2008b). RIM1alpha and RIM1beta are synthesized from distinct promoters of the RIM1 gene to mediate differential but overlapping synaptic functions. J. Neurosci. *28*, 13435–13447.

Kaeser, P.S., Deng, L., Wang, Y., Dulubova, I., Liu, X., Rizo, J., and Südhof, T.C. (2011). RIM proteins tether Ca2+ channels to presynaptic active zones via a direct PDZ-domain interaction. Cell *144*, 282–295.

Kang, M.G., Nuriya, M., Guo, Y., Martindale, K.D., Lee, D.Z., and Huganir, R.L. (2012). Proteomic analysis of α-amino-3-hydroxy-5-methyl-4-isoxazole propionate receptor complexes. J. Biol. Chem. *287*, 28632–28645.

Kavalali, E.T. (2015). The mechanisms and functions of spontaneous neurotransmitter release. Nat. Rev. Neurosci. *16*, 5–16.

Kunz, P.A., Roberts, A.C., and Philpot, B.D. (2013). Presynaptic NMDA receptor mechanisms for enhancing spontaneous neurotransmitter release. J. Neurosci. *33*, 7762–7769.

Larsen, R.S., and Sjöström, P.J. (2015). Synapse-type-specific plasticity in local circuits. Curr. Opin. Neurobiol. *35*, 127–135.

Larsen, R.S., Corlew, R.J., Henson, M.A., Roberts, A.C., Mishina, M., Watanabe, M., Lipton, S.A., Nakanishi, N., Pérez-Otaño, I., Weinberg, R.J., and Philpot, B.D. (2011). NR3A-containing NMDARs promote neurotransmitter release and spike timing-dependent plasticity. Nat. Neurosci. *14*, 338–344.

Maheux, J., Froemke, R.C., and Sjöström, P.J. (2015). Functional plasticity at dendritic synapses. In Dendrites, G. Stuart, N. Spruston, and M. Häusser, eds. (Oxford University Press), pp. 465–498.

Markram, H., Lübke, J., Frotscher, M., Roth, A., and Sakmann, B. (1997). Physiology and anatomy of synaptic connections between thick tufted pyramidal neurones in the developing rat neocortex. J. Physiol. *500*, 409–440.

McGuinness, L., Taylor, C., Taylor, R.D., Yau, C., Langenhan, T., Hart, M.L., Christian, H., Tynan, P.W., Donnelly, P., and Emptage, N.J. (2010). Presynaptic NMDARs in the hippocampus facilitate transmitter release at theta frequency. Neuron *68*, 1109–1127.

Melom, J.E., Akbergenova, Y., Gavornik, J.P., and Littleton, J.T. (2013). Spontaneous and evoked release are independently regulated at individual active zones. J. Neurosci. *33*, 17253–17263.

Nabavi, S., Kessels, H.W., Alfonso, S., Aow, J., Fox, R., and Malinow, R. (2013). Metabotropic NMDA receptor function is required for NMDA receptor-dependent long-term depression. Proc. Natl. Acad. Sci. USA *110*, 4027–4032.

Neher, E. (2015). Merits and limitations of vesicle pool models in view of heterogeneous populations of synaptic vesicles. Neuron *87*, 1131–1142.

Nisticò, R., Florenzano, F., Mango, D., Ferraina, C., Grilli, M., Di Prisco, S., Nobili, A., Saccucci, S., D'Amelio, M., Morbin, M., et al. (2015). Presynaptic c-Jun N-terminal Kinase 2 regulates NMDA receptor-dependent glutamate release. Sci. Rep. *5*, 9035.

Paoletti, P., Bellone, C., and Zhou, Q. (2013). NMDA receptor subunit diversity: impact on receptor properties, synaptic plasticity and disease. Nat. Rev. Neurosci. *14*, 383–400.

Pologruto, T.A., Sabatini, B.L., and Svoboda, K. (2003). ScanImage: flexible software for operating laser scanning microscopes. Biomed Eng. Online Published May 17, 2003. https://doi.org/10.1186/1475-925X-2-13.

Reese, A.L., and Kavalali, E.T. (2016). Single synapse evaluation of the postsynaptic NMDA receptors targeted by evoked and spontaneous neurotransmission. eLife *5*, 5.

Schneggenburger, R., Meyer, A.C., and Neher, E. (1999). Released fraction and total size of a pool of immediately available transmitter quanta at a calyx synapse. Neuron *23*, 399–409.

Schneider, C.A., Rasband, W.S., and Eliceiri, K.W. (2012). NIH Image to ImageJ: 25 years of image analysis. Nat. Methods *9*, 671–675.

Schoch, S., Castillo, P.E., Jo, T., Mukherjee, K., Geppert, M., Wang, Y., Schmitz, F., Malenka, R.C., and Südhof, T.C. (2002). RIM1alpha forms a protein scaffold for regulating neurotransmitter release at the active zone. Nature *415*, 321–326.

Sjöström, P.J., Turrigiano, G.G., and Nelson, S.B. (2003). Neocortical LTD via coincident activation of presynaptic NMDA and cannabinoid receptors. Neuron *39*, 641–654.

Sjöström, P.J., Turrigiano, G.G., and Nelson, S.B. (2007). Multiple forms of long-term plasticity at unitary neocortical layer 5 synapses. Neuropharmacology *52*, 176–184.

Sparks, D.W., and Chapman, C.A. (2014). Contribution of Ih to the relative facilitation of synaptic responses induced by carbachol in the entorhinal cortex during repetitive stimulation of the parasubiculum. Neuroscience *278*, 81–92.

Stocca, G., and Vicini, S. (1998). Increased contribution of NR2A subunit to synaptic NMDA receptors in developing rat cortical neurons. J. Physiol. *507*, 13–24.

Südhof, T.C. (2012). The presynaptic active zone. Neuron *75*, 11–25.

Szczepankiewicz, B.G., Kosogof, C., Nelson, L.T., Liu, G., Liu, B., Zhao, H., Serby, M.D., Xin, Z., Liu, M., Gum, R.J., et al. (2006). Aminopyridine-based c-Jun N-terminal kinase inhibitors with cellular activity and minimal cross-kinase activity. J. Med. Chem. *49*, 3563–3580.

Tang, A.H., Chen, H., Li, T.P., Metzbower, S.R., MacGillavry, H.D., and Blanpied, T.A. (2016). A trans-synaptic nanocolumn aligns neurotransmitter release to receptors. Nature *536*, 210–214.

Tsodyks, M.V., and Markram, H. (1997). The neural code between neocortical pyramidal neurons depends on neurotransmitter release probability. Proc. Natl. Acad. Sci. USA *94*, 719–723.

Watt, A.J., Sjöström, P.J., Häusser, M., Nelson, S.B., and Turrigiano, G.G. (2004). A proportional but slower NMDA potentiation follows AMPA potentiation in LTP. Nat. Neurosci. *7*, 518–524.

Woodhall, G., Evans, D.I., Cunningham, M.O., and Jones, R.S. (2001). NR2B-containing NMDA autoreceptors at synapses on entorhinal cortical neurons. J. Neurophysiol. *86*, 1644–1651.

Yamasaki, T., Kawasaki, H., and Nishina, H. (2012). Diverse roles of JNK and MKK pathways in the brain. J. Signal Transduct. Published online February 8, 2012. https://doi.org/10.1155/2012/459265.

STAR★METHODS

KEY RESOURCES TABLE

REAGENT or RESOURCE	SOURCE	IDENTIFIER
Antibodies		
Anti-RIM1	Proteintech	24576-1-AB
Anti-PSD95	Thermo Fisher Scientific	Cat#MA1-046, RRID: AB_2092361
Anti-vGlut1	Neuromab	Cat#73-066, RRID: AB_10673111
Anti-GluN1	Millipore	05-432
Anti-GluN2B	Millipore	06-600
Anti-GAPDH	Abcam	Cat# ab9484, RRID: AB_307274
Chemicals, Peptides, and Recombinant Proteins		
D/L-AP5	Sigma-Aldrich	A5282
SP600125	Sigma Aldrich	S5567
(+)-MK-801 maleate	Hello Bio	HB0004
TCS JNK 6o	R&D Systems	3222
Ro 25-6981 maleate	R&D Systems	1594
Fluo-5F, pentapotassium salt	Life Technologies	F14221
Alexa 594 hydrazide	Life Technologies	A10438
Critical Commercial Assays		
HotStarTaq DNA Polymerase kit	QIAGEN	203203
Experimental Models: Organisms/Strains		
C57BL/6	The Jackson Laboratory	RRID: IMSR_JAX:000664
$Emx1^{IRESCre/IRESCre}$	The Jackson Laboratory	RRID: IMSR_JAX:005628
Ai9 reporter mice	The Jackson Laboratory	RRID: IMSR_JAX:007909
$RIM1\alpha\beta^{fl/fl}$	Pascal Kaeser, Dept. of Neurobiology, Harvard University, MA	N/A
Oligonucleotides		
RIM1 primers	The Jackson Laboratory	12061, 12062
Emx1 primers	The Jackson Laboratory	oIMR1084, oIMR1085, oIMR4170, oIMR4171
Software and Algorithms		
ScanImage	http://scanimage.vidriotechnologies.com	v3.5-3.7
ImageJ	https://imagej.nih.gov/ij/	v1.50i
Short-term plasticity Bayesian inference method	http://senselab.med.yale.edu/modeldb/showmodel.asp?model=149914	Costa et al., 2013

CONTACT FOR REAGENT AND RESOURCE SHARING

Further information and requests for resources and reagents should be directed to and will be fulfilled by the Lead Contact, Jesper Sjöström (jesper.sjostrom@mcgill.ca).

EXPERIMENTAL MODEL AND SUBJECT DETAILS

Procedures conformed to the *Canadian Council on Animal Care* as overseen by the Montreal General Hospital *Facility Animal Care Committee* and to the *UK Animals (Scientific Procedures) Act 1986*, with appropriate licenses. Male or female P11-P18 mice were anaesthetized with isoflurane and sacrificed once the hind-limb withdrawal reflex was lost. Transgenic animals had no abnormal phenotype. WT animals were predominantly C57BL/6 (000664, The Jackson Laboratory), although a subset was of the GIN strain

(003718, The Jackson Laboratory). Homozygous Emx1$^{IRESCre/IRESCre}$ mice (Gorski et al., 2002) were obtained from The Jackson Laboratory (005628); these are referred to as Emx1$^{Cre/Cre}$ mice for brevity. Homozygous RIM1$\alpha\beta^{fl/fl}$ mice (Kaeser et al., 2008b) were kindly gifted by Pascal Kaeser (Dept of Neurobiology, Harvard University, MA). Heterozygous Emx1$^{Cre/+}$;RIM1$\alpha\beta^{fl/+}$ mice in Figure 4 were generated by crossing Emx1$^{Cre/Cre}$ (Gorski et al., 2002) with RIM1$\alpha\beta^{fl/fl}$ mice (Kaeser et al., 2008b). Emx1$^{Cre/+}$;RIM1$\alpha\beta^{+/+}$, $^{fl/+}$, and $^{fl/fl}$ mice in Figures 5, 6, 7, S4, and S6–S8 were generated by crossing Emx1$^{Cre/Cre}$;RIM1$\alpha\beta^{fl/+}$ mice with RIM1$\alpha\beta^{fl/+}$;no-Cre mice. These distributed in a Mendelian fashion and had viability indistinguishable from that of C57BL/6 mice. Genotyping was carried out using standard methodology with Jackson Laboratory primers (RIM1: 12061, 12062; Emx1: oIMR1084, oIMR1085, oIMR4170, oIMR4171) using QIAGEN HotStarTaq DNA Polymerase kit (203203) and dNTPs from Invitrogen/Thermo-Fisher (18427-013). TdTomato cell counts (Figure S5) were carried out in animals generated by crossing homozygous Ai9 reporter mice (007909, The Jackson Laboratory) with Emx1$^{Cre/Cre}$ mice.

METHOD DETAILS

Slice Preparation and Basic Electrophysiology

Mouse brains were dissected in ice-cold (~4°C) artificial cerebrospinal fluid (ACSF, in mM: NaCl, 125; KCl, 2.5; $MgCl_2$, 1; NaH_2PO_4, 1.25; $CaCl_2$, 2; $NaHCO_3$, 26; Dextrose, 25; bubbled with 95% O_2/5% CO_2). Three-hundred-micron-thick near-coronal slices were cut from visual cortex with a MicroM, Leica VT1200S, or Campden Instruments 5000mz-2 vibratome, according to standard procedures (Abrahamsson et al., 2016). Slices were transferred to an incubation chamber, kept at 37°C up to 1 hr, and then cooled to room temperature (~23°C). Experiments were carried out with ACSF heated to 32-34°C with a resistive inline heater (Scientifica Ltd), with temperature recorded and verified offline. Recordings were truncated if outside this range, or not used at all.

Using a P-97 or a P-1000 electrode puller (Sutter Instruments, Novato, CA, USA), patch pipettes of 4-6 MΩ resistance were pulled from medium-wall capillaries. Pipettes were filled with internal solution consisting of (in mM): KCl, 5; K-Gluconate, 115; K-HEPES, 10; MgATP, 4; NaGTP, 0.3; Na-Phosphocreatine, 10; and 0.1% w/v Biocytin, adjusted with KOH to pH 7.2-7.4. For 2PLSM (see below), internal solution was supplemented with 10-40 μM Alexa Fluor 594 and/or 180 μM Fluo-5F pentapotassium salt (Life Technologies, Carlsbad, CA). Osmolality of internal solution was adjusted to 310 mOsm with sucrose, and the ACSF to 338 mOsm with dextrose (Abrahamsson et al., 2016).

Whole-cell recordings were obtained using BVC-700A (Dagan Corporation, Minneapolis, MN) or MultiClamp 700B amplifiers (Molecular Devices, Sunnyvale, CA). Current clamp recordings were filtered at 5-6 kHz and acquired at 10 kHz using PCI-6229 boards (National Instruments, Austin, TX) with custom software (Sjöström et al., 2003) running in Igor Pro 6 or 7 (WaveMetrics Inc., Lake Oswego, OR) on Dell (Dell Computers, Round Rock, TX) or SuperLogics (Natick, MA) computers. Voltage clamp mini recordings (unfiltered with BVC-700A amplifiers) were additionally software filtered offline at 2 kHz with 6 to 12 pole Butterworth filter (Igor Pro). Series resistance, perfusion temperature, input resistance, resting membrane potential or holding current, and EPSP/C amplitude, as applicable, were monitored online and assessed offline (see below). Series resistance was not compensated. Liquid junction potential (10 mV) was not accounted for.

Neurons were patched at 400x or 600x magnification with infrared video Dodt contrast (Luigs and Neumann, Ratingen, Germany; or built in-house from Thorlabs parts) on custom-modified microscopes (SliceScope, Scientifica Ltd UK, or Olympus BX51WI, Olympus, Melville, NY) (for details, see Buchanan et al., 2012). Primary visual cortex was targeted based on the presence of layer 4. L5 PCs were targeted based on their large somata and conspicuous thick apical dendrites and distinctive triangular shape. Cell morphology was verified using 2PLSM of Alexa 594 fluorescence (e.g., Figure 2A).

Evoked Release

To compensate for the sparse connectivity of L5 PCs (Table S1), we used quadruple whole-cell recordings to test for 12 possible connections simultaneously (Abrahamsson et al., 2016). Seals were formed with four cells and then broken through in rapid succession. To find connections, five spikes were evoked at 30 Hz by 5-ms-long current injections (~1.3 nA) every 10-20 s for ~10 repetitions. Spikes in different cells were separated by >700 ms to ensure that long-term plasticity was not accidentally induced (Sjöström et al., 2003). If no EPSPs were found, all four recordings were discontinued, and another four nearby cells were patched with fresh pipettes. If at least one sufficiently large connection was found (>~0.3 mV, to ensure good signal-to-noise ratio), the baseline of the experiment was started. With extracellular stimulation experiments, stimulating electrodes were pulled from large patch pipettes (tip diameters 2-10 μm) and were filled with ACSF. The stimulating electrode was positioned in L5 under visual guidance, 20-100 μm from the recorded L5 cells. Extracellular stimulation was chiefly used to obtain pilot data relatively quickly. With extracellular stimulation, the identity of the presynaptic cell cannot be known, so the synapse type is not established. Given the synapse-type-specificity of preNMDARs (Blackman et al., 2013; Brasier and Feldman, 2008; Buchanan et al., 2012; Larsen and Sjöström, 2015), this is a possible caveat, which is why the bulk of experiments were done with paired recordings. However, as no differences were found, extracellular stimulation data was pooled with paired recordings (detailed in Figures 1 and 3).

In current-clamp experiments (Figures 1, 5, and 8), bursts of five spikes at 30 Hz were evoked every 20 s. Input resistances, resting membrane potentials, and EPSP amplitudes were continuously monitored online. If these measures were deemed stable, wash in of either AP5 or Ro was commenced after 10–15 min. The spike bursts were continued up to 200 repetitions for a total of 67 min. AP5 was present for 10 min, whereas Ro was present for the duration of the recording, as GluN2B-specific blockers such as Ro

(Buchanan et al., 2012) and ifenprodil (Sjöström et al., 2003) cannot reliably be washed out. The slice was replaced after each Ro treatment. In NMDA:AMPA ratio current-clamp experiments (Figure 5 and associated main text), the AMPAR component was measured in a 1-ms window set at a fixed latency of 2-4 ms, whereas the NMDAR component was measured at a 15 to 20-ms-long window starting 15 ms after the presynaptic action potential, and ending before the second response in a 30-Hz train (see Watt et al., 2004).

In SMN RRP depletion experiments (Figures 3 and 4) (Schneggenburger et al., 1999), we searched for connected pairs of neurons in current clamp as described above. Once found, the postsynaptic cell was voltage clamped at −80 mV. Next, the RRP was depleted using burst of 14 spikes at 30 Hz repeated every 80 s, while the postsynaptic cell was temporarily clamped to −90 mV with a 3 s-long voltage step. We settled on this protocol because it was stable (Figures 3C–3F) — we tried higher burst frequencies, or a repetition rate of every 40 s, but both led to EPSC rundown (data not shown). As above, input resistances, resting membrane potentials, and EPSC amplitudes were continuously monitored. However, the pre-drug baseline period was fixed to 15 repeats, or 20 min. AP5 was temporarily washed in for 16 repeats (21.33 min), whereas Ro was present for the duration of the recording once washed in. The slice was replaced after each Ro treatment.

We used quality selection criteria similar to those we used before (Buchanan et al., 2012; Sjöström et al., 2003). Input and series resistance were assessed with a 250-ms-long test pulse that was −25 pA in current clamp and −5 mV in voltage clamp. Recordings with more than 30% change in input resistance or more than 8 mV change in resting membrane potential were discarded or truncated. Voltage-clamp recordings for which series resistance exceeded 40 MΩ or changed more than 20% were discarded or truncated. Recordings shorter than 20 min after commencing drug wash-in were not used. Experiments with unstable baseline, as assessed using a t test of Pearson's r for response amplitude over time, were discarded. With AP5 wash-in experiments, we additionally required that responses at least temporarily recovered to within 10% of the baseline response amplitude, or else the recording was discarded.

Evoked responses were averaged during baseline and drug conditions. PreNMDAR-mediated suppression of evoked neurotransmission was expressed in terms of the ratio of the first response in a train averaged over drug wash-in divided by that averaged over the pre-drug baseline period, as indicated (e.g., Figures 1A and 1B). To measure short-term plasticity, we used the paired-pulse ratio, PPR, defined as $(R_2\text{-}R_1)/R_1$, where R_i is the i^{th} response in a 30-Hz train. Although trains of five or fourteen responses were always employed (except for at 0.1 Hz in Figure 1C, where only one response was used), we previously found that using R_3 and beyond did not appreciably affect the short-term plasticity analysis (see Sjöström et al., 2007). The change in paired-pulse ratio, ΔPPR, was calculated as $PPR_{drug} - PPR_{baseline}$. CV analysis was carried out as previously described (see Buchanan et al., 2012; Sjöström et al., 2007). R_1 mean and R_1 CV were calculated from baseline and drug conditions. The CV was corrected for background noise. Mean and CV^{-2} were normalized to the baseline period. The angle between the diagonal and the line defined by the starting point at coordinate (1,1) and the CV analysis endpoint was used to define the measure φ (see Figure 3G). A postsynaptic locus was thus indicated by $\varphi < 0$, while $\varphi > 0$ indicated a presynaptic effect.

We verified that enough glutamate was released to activate preNMDARs in hetero- and homozygous RIM1αβ KO mice. If the amount of glutamate released determined preNMDAR efficacy, then there should be a correlation between Ro-mediated suppression of neurotransmission and initial release. However, the effect of Ro wash-in on EPSC amplitude was not correlated with initial paired-pulse ratio (Pearson's r = 0.015, p = 0.97, n = 11) or with baseline EPSC amplitude (r = −0.287, p = 0.39, data not shown), arguing against this possibility. In agreement, very low-p_r synapses from L5 PCs to Martinotti cells were also sensitive to preNMDAR blockade (Buchanan et al., 2012), indicating that a lack of glutamate spillover in RIM1αβ KO mice cannot cause preNMDAR signaling to malfunction. Finally, spontaneous release was also sensitive to preNMDAR blockade (Figure 2), showing that either ambient glutamate or individual vesicles contain enough glutamate to activate preNMDARs.

Spontaneous Release

Spontaneous release was recorded in voltage clamp to −80 mV in the presence of 0.1 μM TTX and 20 μM Bicuculline. The ACSF and internal solution were otherwise as described above, except the internal solution was supplemented with 2 mM MK-801 in Figures 2G–2I (Buchanan et al., 2012; Woodhall et al., 2001). 25-s-long sweeps were acquired every 30 s and were low-pass filtered offline at 2 kHz using a 6-12 pole Bessel filter (Igor Pro). Minis were automatically detected with detection criteria including amplitude > 5 pA and rise time < 3 ms (Buchanan et al., 2012). Minis with overlap or unstable baselines were automatically discarded. The occasional sweep with large artifacts due to e.g., electrical noise were manually discarded. Recordings with <1 Hz initial mini frequency were not used, except for in P3-P5 animals (Figure S1), for which the mini frequency was typically lower. Ensemble average time courses (e.g., Figures 2C and 2E) were normalized to baseline period. As with evoked release experiments (above), input and series resistance were assessed with a −5 mV 250-ms-long test pulse. Recordings with more than 30% input resistance change, series resistance exceeding 40 MΩ, or series resistance changing more than 20% were discarded or truncated. Recordings shorter than 20 min after start of drug wash-in were rejected. Experiments with unstable baseline were not used, with stability measured using a t test of Pearson's r for mini frequency over time. AP5 experiments were furthermore required to recover to within 10% of the baseline frequency.

For the NMDA:AMPA ratio experiments (Figures S1 and S2), the ACSF $MgCl_2$ concentration was additionally lowered to 0.2 mM. Also, we used cesium-based internal solution, containing (in mM): Cs-gluconate, 100; CsCl, 5; HEPES, 10; MgATP, 4; NaGTP, 0.3; Na-Phosphocreatine, 10; NaCl, 8; QX-314, 5; TEA, 5, adjusted with CsOH to pH 7.2-7.4. The AMPA current was measured at the peak of the mini, whereas the NMDA component was measured in a 10-ms-long window 20 ms after the peak.

Pharmacology

D/L-AP5 (Sigma-Aldrich, R & D Systems, Cedarlane, or Hello Bio) was used at 200 μM. Ro 25-6981 maleate (R & D Systems, Cedarlane, Fisher Scientific, or Hello Bio) was used at 0.5 or 5 μM. External MK-801 maleate (Hello Bio) was washed in at 2 μM (Sjöström et al., 2003; Reese and Kavalali, 2016), but internally loaded at 2 mM (Buchanan et al., 2012; Woodhall et al., 2001). In JNK2 blockade experiments, slices were incubated (but not dissected) in ACSF containing 4 μM SP600125 (Sigma-Aldrich, Hello Bio) for at least 2 hr before the start of recordings, and perfusion ACSF was also supplemented with SP600125. TCS JNK 6o (R & D Systems) was used in the same manner, but at 0.1 μM concentration.

2PLSM and Uncaging

2PLSM was performed with imaging workstations custom-built from BX51WI (Olympus, Melville, NY) or SliceScope (Scientifica Ltd, UK) microscopes (described in detail in Buchanan et al., 2012). Briefly, detectors were based on R3896 bialkali photomultipliers (Hamamatsu, Bridgewater, NJ) and scanners were 6215H 3-mm galvanometric mirrors (Cambridge Technology, Bedford, MA). For uncaging experiments, detectors were in substage configuration, to allow the 405-nm laser beam to reach to the acute slice. Two-photon excitation was achieved using a Chameleon XR (Coherent, Santa Clara, CA, USA) or MaiTai HP (Spectraphysics, Santa Clara, CA, USA) titanium-sapphire laser tuned to 800-820 nm. Lasers were gated with SH05/SC10 (Thorlabs) or Uniblitz LS6ZM2/VCM-D1 (Vincent Associates, Rochester, NY, USA) shutters, and manually attenuated with a polarizing beam splitter in combination with a half-lambda plate (Thorlabs GL10-B and AHWP05M-980). Laser output was monitored with a power meter (Thorlabs PM100A with S121C; or Newport 1916-R with 818-SL). Fluorescence was collected with an FF665 dichroic and an FF01-680/SP-25 emitter (Semrock Inc., Rochester, NY, USA). Red and green fluorescence were separated with a t565lpxr (Chroma, Bellow Falls, VT, USA) or a FF560-Di01 dichroic beam mirror (Semrock), a ET630/75 m (Chroma) red emitter, and a ET525/50 m (Chroma) or a FF01-525/45-25 (Semrock) green emitter. Laser-scanning Dodt contrast was achieved by collecting the laser light after the spatial filter with an amplified diode (Thorlabs PDA100A-EC). In uncaging experiments, the 405-nm laser was blocked from reaching the detector using a long-pass filter (Semrock BLP01-488R-25). Imaging data were acquired using customized variants of ScanImage version 3.5–3.7 (Pologruto et al., 2003) running in MATLAB (The MathWorks, Natick, MA, USA) via PCI-6110 boards (National Instruments).

After each whole-cell recording, L5 PC morphologies were acquired as stacks of 512-by-512-pixel slices separated by 1-2 μm (1.5 pixels/μm). Each slice was an average of 2-4 red-channel frames acquired at 2 ms per line. Morphologies shown (e.g., Figure 2A) are pseudo-colored maximum-intensity projections of such 3D stacks. Spine counts were carried out using ImageJ v1.50i on 256-by-256-pixel stacks acquired at zoom 5 (~3.75 pixels/μm) with a slice separation of 2 μm, with each slice being an average of three red-channel frames. Spine counts were done blinded to condition.

Ca^{2+} imaging was started >1 hr after break-through, to permit dye wash in and equilibration. Ca^{2+} signals were measured as change in green Fluo-5F fluorescence normalized to red Alexa-594 fluorescence (dG/R). Linescans were acquired at 128 pixels and 1 ms per line for a duration of 512-1024 ms each. Electrophysiology and imaging were synchronized by external triggering.

Uncaging was achieved with a 150-mW 405-nm violet solid-state laser (MonoPower-405-150-MM-TEC, Alphalas GmbH, Göttingen, Germany) that was gated with the built-in trigger. The violet uncaging beam was combined with the 2-photon imaging beam using a dichroic (Semrock FF665-Di02) so that both beams were scanned with the same 6215H mirror set. The galvanometric scanners were temporarily parked at the center of the screen for the duration of the uncaging pulse, and the imaged region of interest was centered. Uncaging laser power was set to max and pulse duration was always 2 ms. Power at the objective back aperture was 6 mW. Axonal boutons were defined as axonal swellings with significant Ca^{2+} signals ($p < 0.05$) due to a 30-Hz burst of spikes, as measured across 5-10 line scans.

ACSF with 1 mM MNI-NMDA and 20 mM Na-HEPES (pH 7) was puffed onto the region of interest using a glass pipette with 4-5 μm diameter tip. MNI-NMDA solutions were handled in the dark or with red LED illumination (Thorlabs LIU001). Microscope lighthouse was long-pass filtered at 780 nm (Thorlabs FGL780). Uncaging laser pulse artifacts were blanked out in imaging data. Three scan conditions *both*, *light*, and *APs* were interleaved, repeating them a minimum of six times each, every 7 s. *APs* denotes a 30-Hz burst of five action potentials, *light* the uncaging pulse, and *both* refers both simultaneously. To avoid accidentally introducing an invalid sub or supralinearity, axonal or dendritic compartments with significant trends in baseline or evoked Ca^{2+} across line scans (t test of Pearson's r) were not used. For clarity, sample Ca^{2+} traces in Figure 5 are filtered averages, but statistics were carried out on individual raw data sweeps.

Computer Modeling

Synaptic dynamics were modeled using the Tsodyks-Markram short-term plasticity model (Tsodyks and Markram, 1997) with short-term depression without facilitation. This model has two key parameters: vesicle usage and tau recovery, where the former corresponds to release probability. This version of the model provides a good description of short-term dynamics at PC connections in developing neocortex (Costa et al., 2013). Synaptic response amplitudes were extracted from experiments before and after drug, Ca^{2+}, or mock wash-in by subtracting fitted exponentials to account for temporal summation (see Sjöström et al., 2007). Short-term plasticity parameters were estimated using a Bayesian inference method as previously described (Costa et al., 2013). Briefly, we used a Markov-chain Monte-Carlo method to estimate the full posterior probability of the Tsodyks-Markram model given the

synaptic response amplitudes. We then compared the maximum *a posteriori* (i.e., the most likely parameter combination) before and after Ro, Ca^{2+}, or mock wash-in (see Figure S3; example inference code available at http://senselab.med.yale.edu/modeldb/showmodel.asp?model=149914).

Western Blotting

We dissected the cortex at P12-16. Whole cell lysates were obtained by homogenizing the cortex in an appropriate volume of RIPA buffer (1% Triton X-100, 1% sodium deoxycholate, 0.1% SDS, 20 mM Tris pH 8.0, 150 mM NaCl and 1 mM EDTA) using a Dounce homogenizer. Lysates were left on ice for 30 min, sonicated for 10 s and spun at 13,200 rpm for 10 min. Supernatants were collected and protein concentration was determined using a BCA assay (Pierce). 20 μg of total protein from each genotype was run on 10% SDS-PAGE gels and subjected to immunoblotting as described above. Membranes were incubated with either anti-RIM1 (Proteintech 24576-1-AB,1:3000), anti-PSD95 (ThermoFischer Scientific MA1-046, 1:100,000); anti-vGlut1(Neuromab 75-066, 1:10,000), anti-GluN1 (Millipore 05-432, 1:5,000), anti-GluN2B (Millipore 06-600, 1:8,000) or anti-GAPDH (Abcam ab9484, 1:50,000) as a loading control.

We used ImageJ (Schneider et al., 2012) to quantify the expression profile of RIM1 relative to GAPDH using densitometry and the ImageJ Gel Analysis Plugin (https://imagej.nih.gov/ij/docs/menus/analyze.html). We first normalized the intensity of the bands for either RIM1, PSD95, vGlut1, GluN2b, GluN1 to GAPDH by dividing the area measurements returned by ImageJ and then expressed the level of expression as a percentage of the WT animals. This was repeated across at least 3 independent experiments.

Co-immunoprecipitation

For the co-immunoprecipitation assay, the cortex was dissected out from WT animals and prepared for GluN2B co-immunoprecipitation using a previously published co-immunoprecipitation buffer containing in PBS: 0.5% Triton X-100, 0.5 mM EDTA, 0.5 mM EGTA and a mixture of protease and phosphatase inhibitors (Kang et al., 2012). Co-immunoprecipitated lysate was then immunoblotted for GluN2B and RIM1 using anti-GluN2b and anti-RIM1 antibodies. Rabbit immunoglobulin co-immunoprecipitated lysate and GAPDH expression were used as negative control for the co-immunoprecipitation assay.

QUANTIFICATION AND STATISTICAL ANALYSIS

Results are reported as mean ± standard error of the mean. For multiple comparisons, two-way comparisons were carried out only if ANOVA permitted it at the $p < 0.05$ level. We used Brown-Forsythe's ANOVA if Bartlett's test indicated unequal variances at the $p < 0.05$ level. Kruskal-Wallis's non-parametric variant was always used in parallel and gave similar significance levels. Unless otherwise specified, two-way comparisons were made using unpaired Student's t test for equal means. If the F test was significant ($p < 0.05$), the unequal variances t test was used. To correct post hoc for multiple comparisons, we utilized the Bonnferoni-Dunn adjustment. Wilcoxon-Mann-Whitney's non-parametric test was always used in parallel and gave similar significance levels. Incidence of supralinearities (Figures 6L and 6M) and connectivity rates (Table S1) were assessed with the chi-square test and the Cochran-Armitage test for trend. The magnitude of supralinearities was assessed with the Kendal tau test as well as with a t test for Pearson's r (Figure 6M). Statistical tests were carried out in Igor Pro, Excel, JMP (SAS, NC), and/or MATLAB. One, two, and three asterisks denote $p < 0.05$, $p < 0.01$, and $p < 0.001$ significance levels, respectively.

Clustering was carried out with custom-written agglomerative single-linkage hierarchical classification software running in Igor Pro (see Figures 6F and 6L), as previously described (Buchanan et al., 2012). The squared Euclidian distance was used as linkage metric, and the best-cut level was set to 50% to determine the clusters.

Neuron, Volume *96*

Supplemental Information

Differential Regulation of Evoked and Spontaneous Release by Presynaptic NMDA Receptors

Therése Abrahamsson, Christina You Chien Chou, Si Ying Li, Adamo Mancino, Rui Ponte Costa, Jennifer Anne Brock, Erin Nuro, Katherine Anne Buchanan, Dale Elgar, Arne Vladimir Blackman, Adam Tudor-Jones, Julia Oyrer, William Todd Farmer, Keith Kazuo Murai, and Per Jesper Sjöström

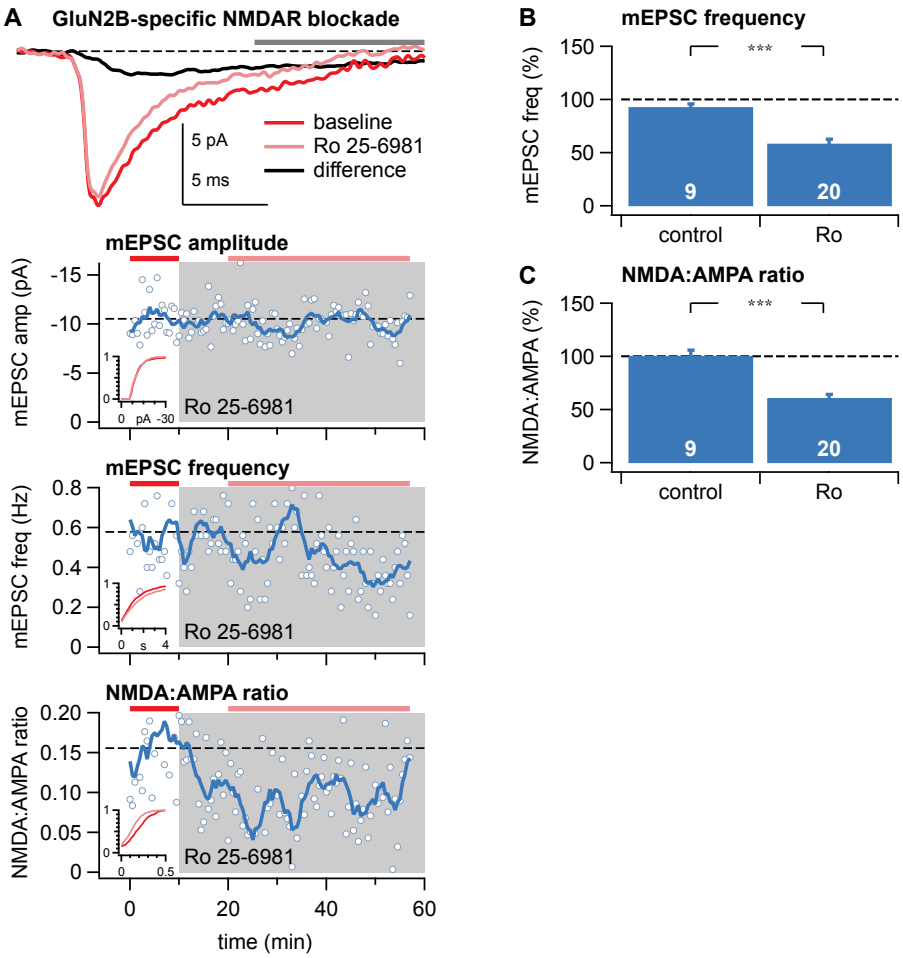

Figure S1. At P3-P5, Postsynaptic NMDARs Contain the GluN2B Subunit, Related to Figure 2

(A) Sample experiment showing that, in 0.2 mM Mg^{++}, wash-in of the GluN2B-specific NMDAR antagonist Ro reduced mini frequency (0.58 ± 0.04 Hz to 0.45 ± 0.02, $p < 0.05$) and NMDA:AMPA ratio (0.16 ± 0.01 to 0.092 ± 0.005, $p < 0.001$) but not amplitude (-11 ± 0.5 pA to -10 ± 0.2 pA, $p = 0.36$) as expected from combined pre- and postsynaptic effects. Top: The difference current (black) is consistent with the relatively slow kinetics of GluN2B-containing NMDAR-mediated current (Paoletti et al., 2013) that affects the peak mini current relatively little. Inset figures: Cumulative histograms.

(B) Ro robustly reduced mini frequency as compared to controls, consistent with the existence of preNMDARs at in L5 PCs from P3-P5 animals. Baseline mini frequency was 0.57 ± 0.06 Hz, n = 29, considerably lower than at P11-P16 (e.g. $p < 0.001$ compared to **Figure S2C**).

(C) At P3-P5 as opposed to at P11-P16 (see **Figure S2**), Ro reduced the NMDA:AMPA ratio, demonstrating that postsynaptic NMDARs in L5 PCs of mouse visual cortex are sensitive to GluN2B-specific blockade, as previously demonstrated in the rat (Stocca and Vicini, 1998). Baseline NMDA:AMPA ratio was 0.18 ± 0.01, n = 29, somewhat higher than at P11-P16 ($p < 0.05$), presumably because currents of NMDAR containing the GluN2B subunit decay more slowly than those with GluN2A (Paoletti et al., 2013).

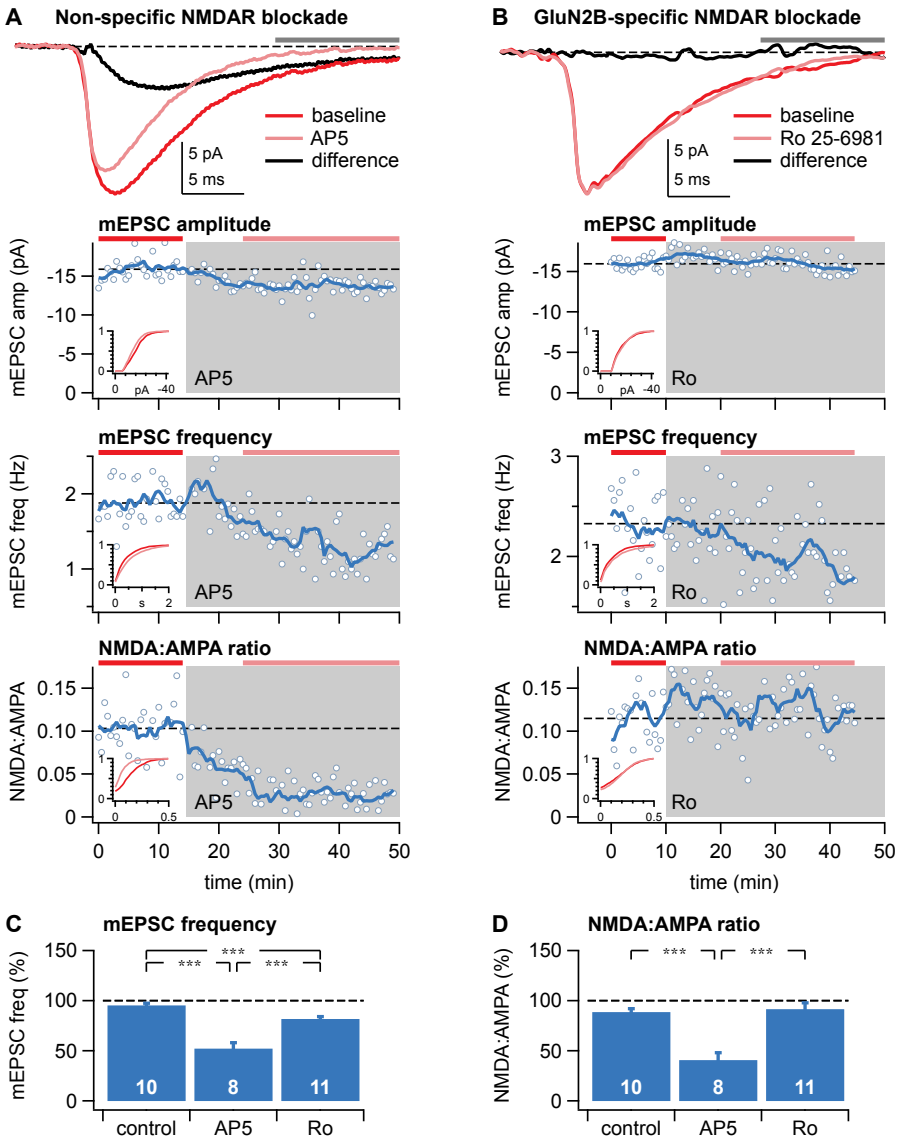

Figure S2. At P11-P16, preNMDARs Contain the GluN2B Subunit whereas Postsynaptic NMDARs do not, Related to Figure 2

(A) Sample experiment in 0.2 mM Mg^{++} to relieve NMDARs of Mg^{2+} block showing that wash-in of the non-specific NMDAR antagonist AP5 reduced mini amplitude (-16 ± 0.3 pA to -14 ± 0.2 pA, $p < 0.001$), frequency (1.9 ± 0.05 Hz to 1.4 ± 0.05 Hz, $p < 0.001$), and NMDA:AMPA ratio (0.10 ± 0.005 to 0.027 ± 0.003, $p < 0.001$) as expected from combined pre- and postsynaptic effects. Top: The difference current (black) is consistent with an NMDAR-mediated current. Inset figures: Cumulative histograms.

(B) Sample recording showing a reduction of mini frequency (2.3 ± 0.08 Hz to 2.0 ± 0.05 Hz, $p < 0.01$) but not amplitude (-16 ± 0.2 pA to -16 ± 0.1 pA, $p = 0.79$) or NMDA:AMPA ratio (0.11 ± 0.007 to 0.13 ± 0.005, $p = 0.19$) due to wash-in of Ro in 0.2 mM Mg^{++}, showing that pre- but not postsynaptic NMDARs are sensitive GluN2B-specific blockade. Top and insets as in (A).

(C) Both AP5 and Ro robustly reduced mini frequency as compared to controls, in agreement with the view that preNMDARs are sensitive to GluN2B-specific blockade (Brasier and Feldman, 2008; Sjöström et al., 2003; Woodhall et al., 2001). The additional reduction of mini frequency due to AP5 results from the mini detection software missing events that drop below the detection threshold (STAR Methods) and does not imply that AP5 blocks preNMDARs better than Ro does. Baseline mini frequency was 2.8 ± 0.2 Hz, n = 29.

(D) AP5 but not Ro reduced the NMDA:AMPA ratio, showing that post- but not presynaptic NMDARs have undergone the GluN2B-to-2A developmental switch in L5 PCs of P11-16 mice, as previously demonstrated in the rat (Stocca and Vicini, 1998) (also see Sjöström et al., 2003). Baseline NMDA:AMPA ratio was 0.14 ± 0.01, $n = 29$.

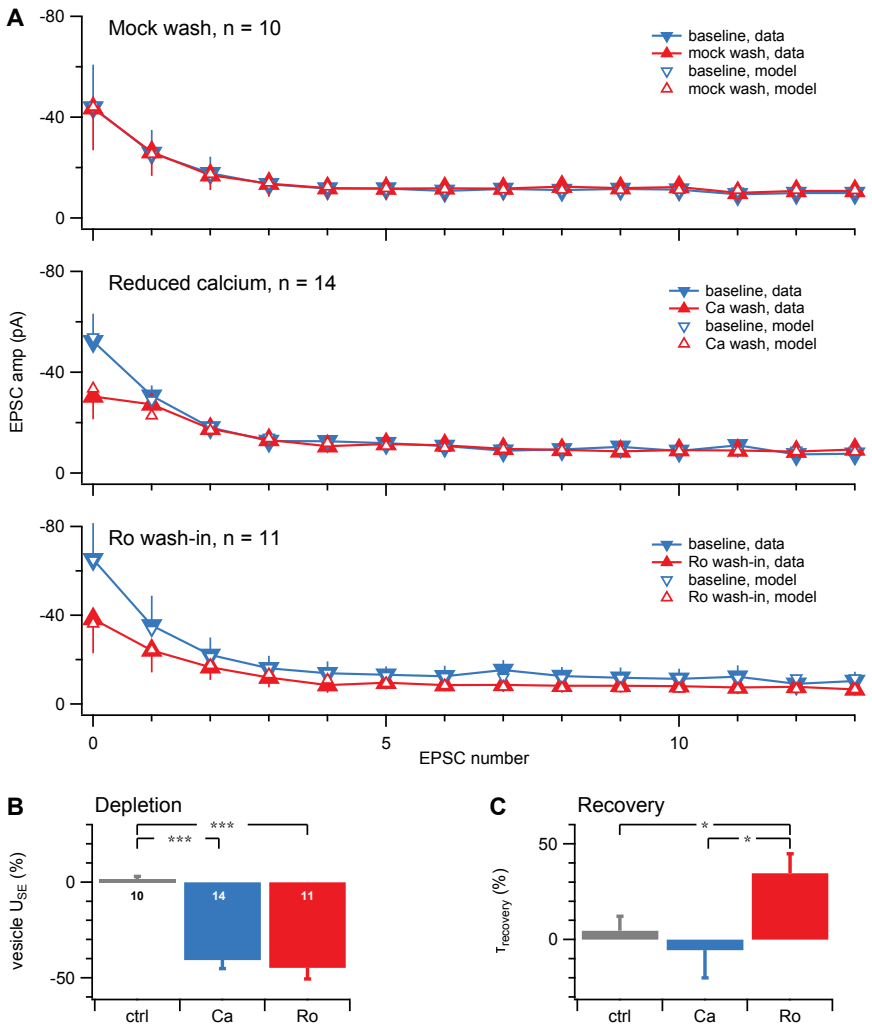

Figure S3. Computer Modelling Supports the Finding that PreNMDARs Regulate RRP Replenishment Rate during Evoked Release, Related to Figure 3

(A) The TM short-term depression model (Tsodyks and Markram, 1997) was fitted (open symbols) using Bayesian inference (see STAR Methods and Costa et al., 2013) to data (closed symbols) from the three conditions: mock wash-in, reduced Ca^{2+}, and Ro wash-in. Note that Ro wash-in (but not lowered Ca^{2+}) reduced the steady-state response amplitude, indicating a decreased RRP replenishment rate.

(B) The vesicle usage parameter U_{SE} was decreased by both lowered Ca^{2+} ("Ca") and by Ro wash-in ("Ro") relative to controls ("ctrl"), implying a reduced p_r in both conditions.

(C) Ro wash-in but not lowered Ca^{2+} increased the recovery time constant $\tau_{recovery}$, demonstrating that Ro wash-in had effects beyond those resulting from reduced Ca^{2+} influx.

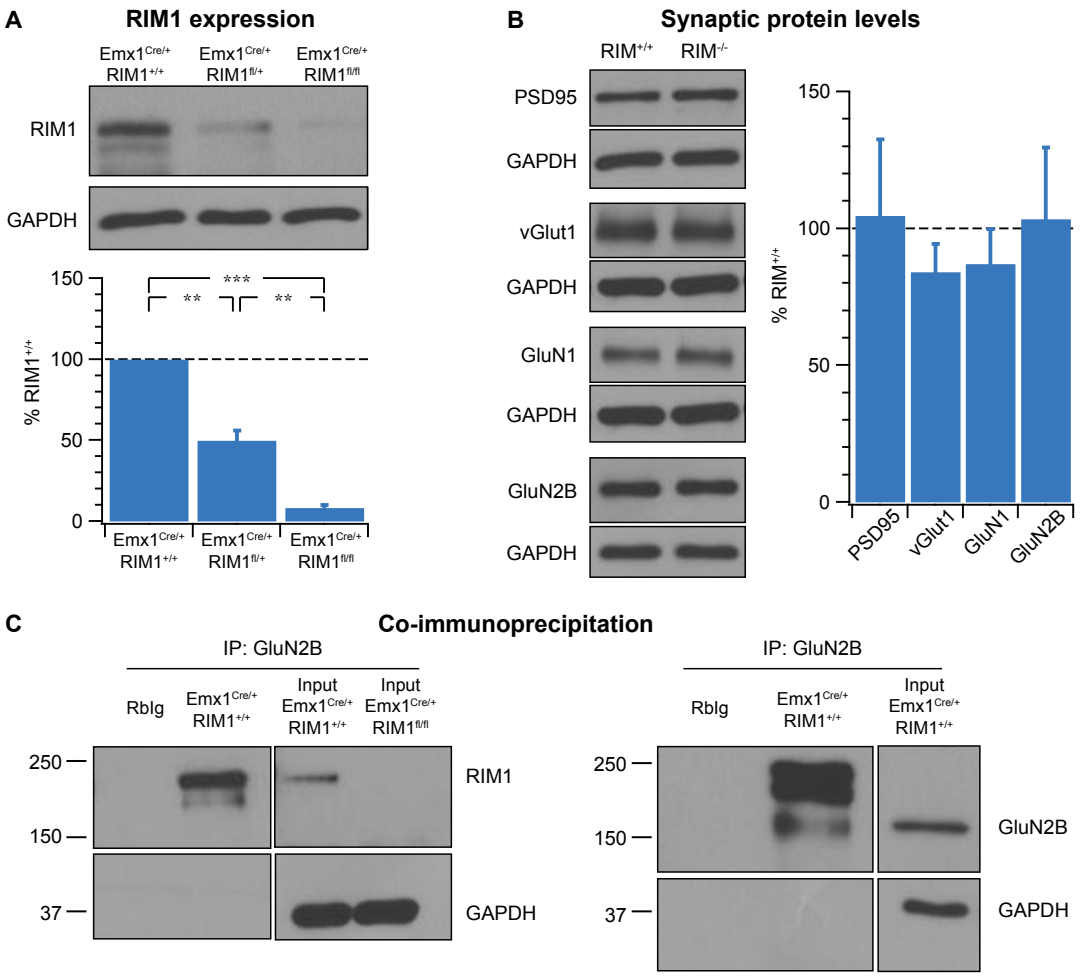

Figure S4. An Association of GluN2B-RIM1 is Evidenced by Characterization of WT and RIM1αβ Knockout Mice, Related to Figure 4

(A) RIM1 expression levels were progressively reduced in cortex of heterozygous and homozygous KO mice (n = 5 animals per condition). Expression was not, however, abolished in cortex from homozygous RIM1 deletion animals, in keeping with the specificity of the Emx1 promoter for PCs (Gorski et al., 2002), which leaves RIM1 intact at inhibitory synapses. As numerical values depend on exposure time, this quantification does not imply that overall 10% of RIM1 is left in homozygous mice, only that gradually less RIM1 is present in homo- and heterozygous deletion mice compared to controls. This graded reduction is consistent with RIM1 haploinsufficiency (see main text).

(B) The expression levels of the key synaptic proteins PSD95, vGlut1, GluN1, and GluN2B were not detectably affected by homozygous RIM1 KO (n = 4 animals per condition, except for GluN2B: n = 3).

(C) Left: GluN2B IP with blotting for RIM1 demonstrates a band of the expected size, consistent with GluN2B and RIM1 being associated in the same complex. Right: GluN2B immunoprecipitation (IP) followed by blotting for GluN2B reveals an appropriately sized band compared to in total lysate (Input). RbIg: Rabbit immunoglobulin negative control. Note that the RIM1 band is stronger than in A, where only 1.5% of input was loaded.

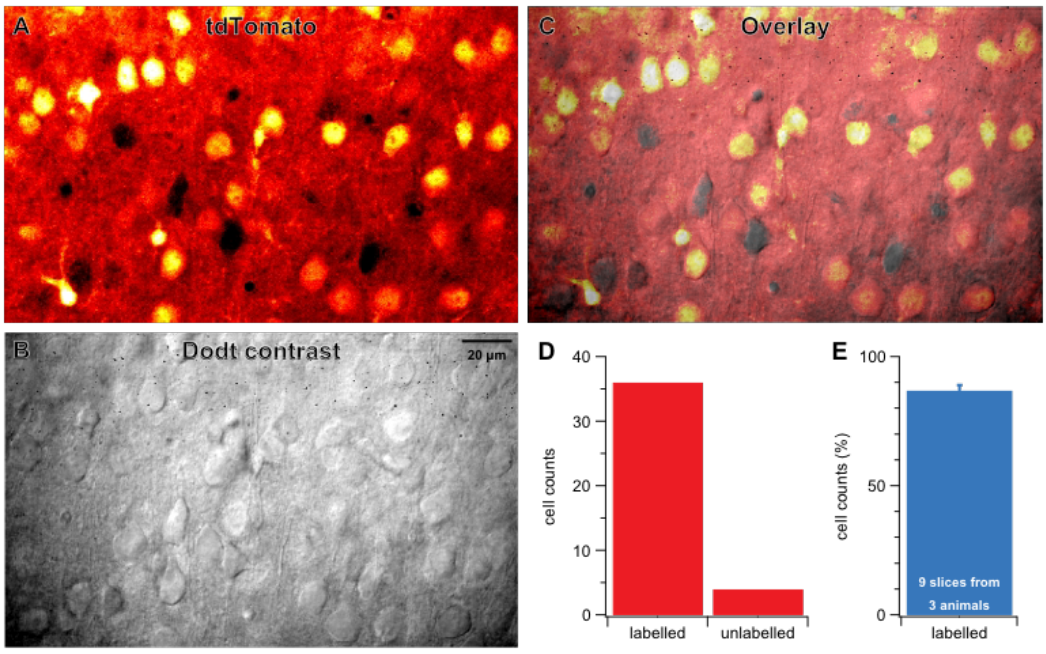

Figure S5. Emx1-Cre Drives Expression in a Majority of Neurons, Related to Figure 4

(A) Sample 2PLSM red-channel image of acute slice from $Emx1^{Cre/+};Ai9^{tdTom/+}$ mice (STAR Methods) showing only a handful of PCs that were not labelled by tdTomato (black pyramid-shaped regions).

(B) Laser-scanning Dodt contrast (STAR Methods) of the same slice illustrates the straight-forward identification of PCs.

(C) Overlay of images in A and B illustrate how labeled versus unlabeled PCs were counted.

(D) Thirty-six of 40 PCs (90%) in the sample image in panels A-C were labelled.

(E) Across 3 mice, 87% ± 2% of cells were labelled. Although the incidence of tdTomato-expressing PCs in $Emx1^{Cre/+};Ai9^{tdTom/+}$ mice need not correspond perfectly to the rates of PCs with RIM1 KO in $Emx1^{Cre/+};RIM1\alpha\beta^{fl/+}$ or $Emx1^{Cre/+};RIM1\alpha\beta^{fl/fl}$ mice, this verifies previous results showing that Emx1 mice drive Cre expression in a majority of neocortical excitatory neurons (Gorski et al., 2002).

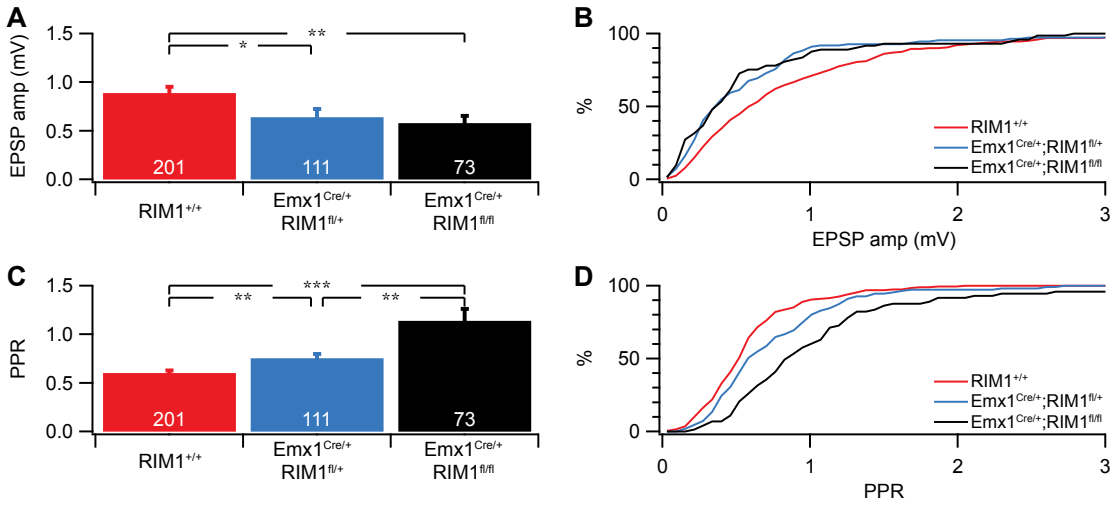

Figure S6. Evoked Release is Reduced in RIM1αβ KO Mice, Related to Figures 4 and 5

Across 385 paired L5 PC recordings, RIM1αβ KO led to smaller EPSP amplitude (A, B) and increased PPR ratio (C, D) in a gene-dosage-dependent manner, in keeping with the previously reported role for RIMs in short-term depression and vesicle priming (Südhof, 2012). $RIM1^{+/+}$ denotes WT, $RIM1\alpha\beta^{fl/fl}$;no-Cre, and $Emx1^{Cre/+}$;$RIM1\alpha\beta^{+/+}$ pooled, as they were indistinguishable (amplitude $p_{ANOVA} = 0.17$ and PPR $p_{ANOVA} = 0.45$; STAR Methods).

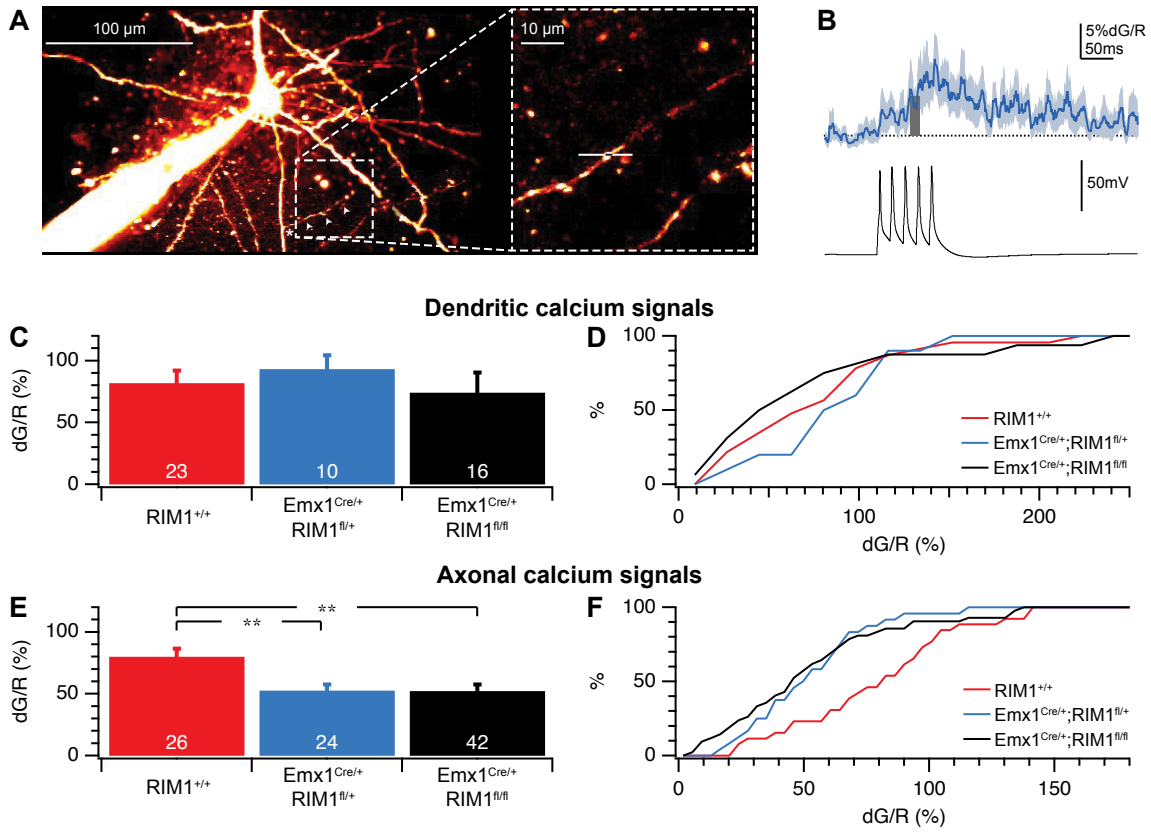

Figure S7. Axonal but not Dendritic Spike-Triggered Ca^{2+} Transients are Reduced in RIM1αβ KO Mice, Related to Figure 6

(A) Sample 2PLSM stack showing an axon collateral (arrow heads) branching off the main axon (asterisk), with position of linescan indicated in inset image.

(B) The spike-evoked Ca^{2+} signal was measured in a 15-ms-long window (grey box) positioned 50 ms after the onset of the current injection (five 5-ms-long current pulses at 50 Hz, see STAR Methods). The Ca^{2+} signal (blue; average of six linescans) was box-filtered at 7 ms for clarity, but signal was measured on unfiltered data.

(C, D) RIM1αβ KO had no effect on spike-mediated Ca^{2+} transients in dendritic compartments, indicating no appreciable role for RIM1 on the postsynaptic side.

(E, F) Ca^{2+} signals were reduced in axonal boutons, in keeping with the previously reported role for RIMs in scaffolding VDCCs (Südhof, 2012). These findings are also consistent with the reduced evoked responses (**Figure S6**). $RIM1^{+/+}$ denotes WT and $Emx1^{Cre/+}$;$RIM1\alpha\beta^{+/+}$ pooled, as no difference was found ($p = 0.31$; STAR Methods).

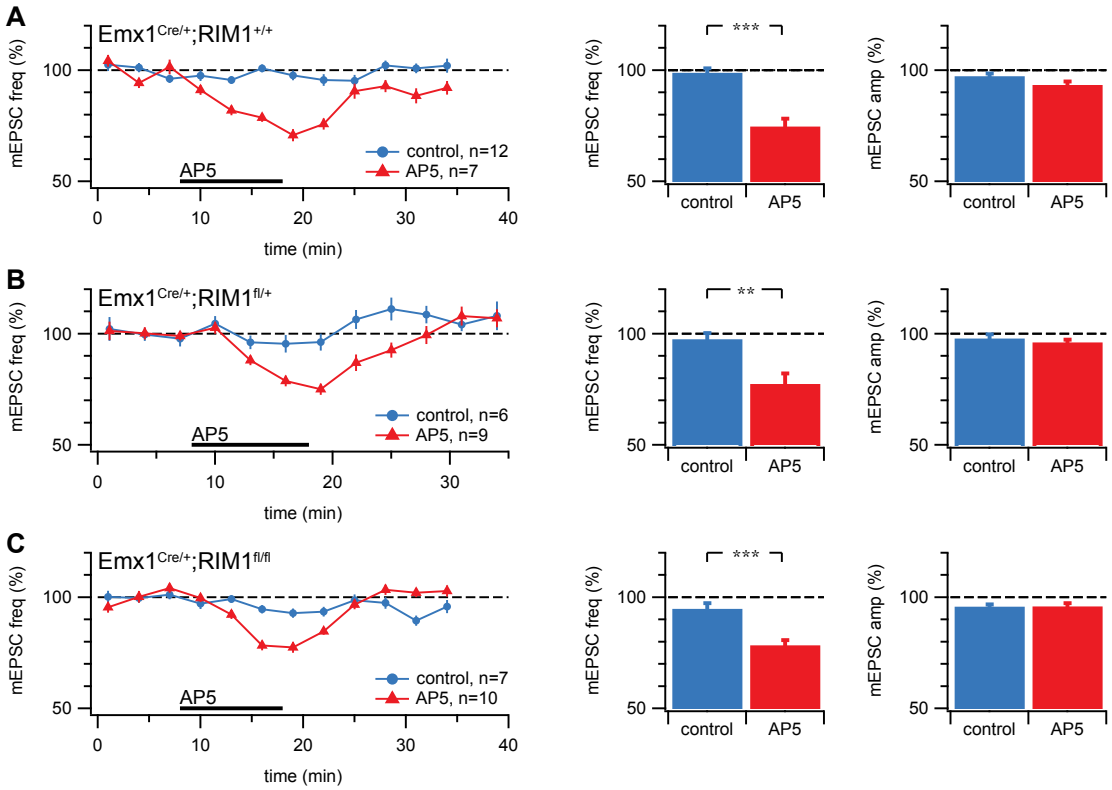

Figure S8. PreNMDAR-Dependent Regulation of Spontaneous Release is Unaffected by RIM1αβ Knockout, Related to Figure 7

AP5 wash-in reversibly reduced mini frequency but not amplitude in Emx1$^{Cre/+}$;RIM1αβ$^{+/+}$ L5 PCs (A, red), as expected from prior findings (**Figure 2**) (Berretta and Jones, 1996; Corlew et al., 2007; Sjöström et al., 2003). Results in heterozygous Emx1$^{Cre/+}$;RIM1αβ$^{+/fl}$ (B, red) or homozygous Emx1$^{Cre/+}$;RIM1αβ$^{fl/fl}$ KO PCs (C, red) were the same, indicating that preNMDAR-mediated regulation of spontaneous release did not directly need RIM1. Mock wash-in controls are shown in blue (A-C).

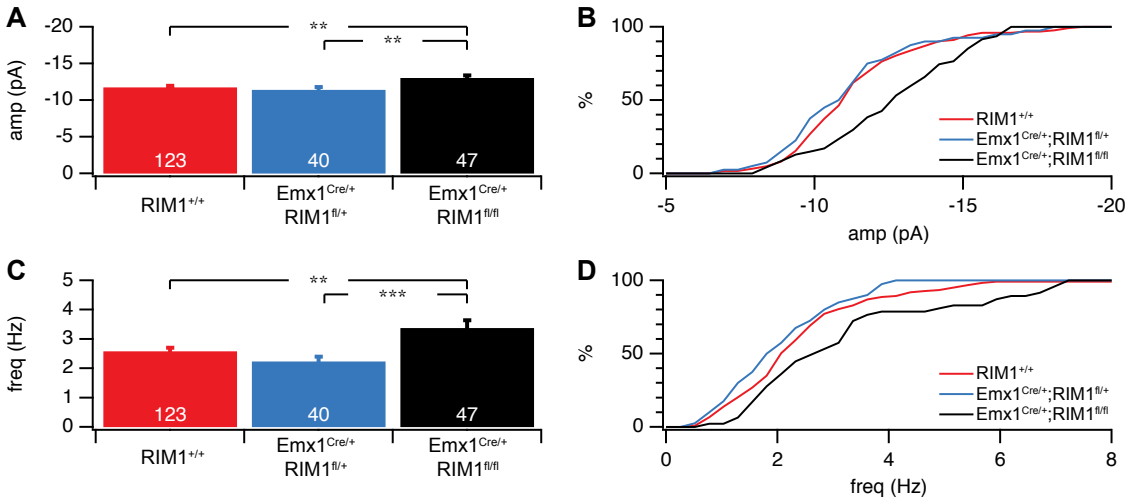

Figure S9. Spontaneous Release is Increased in Homozygous RIM1αβ KO Mice, Related to Figure 7

Homozygous but not heterozygous RIM1αβ KO led to larger mini amplitude (A, B) and frequency (C, D). $RIM1^{+/+}$ denotes $RIM1\alpha\beta^{fl/fl}$;no-Cre and $Emx1^{Cre/Cre}$ pooled, as they were not different (amplitude $p_{ANOVA} = 0.94$ and frequency $p_{ANOVA} = 0.89$; STAR Methods).

Table S1. PC-PC Connectivity Rates were Unaffected by RIM1αβ KO, Related to Figure 7

Category	Connections found	Pairs tested	Connectivity rate (%)	Number of cells
$RIM^{+/+}$	415	2976	13.9%	2473
$Emx1^{Cre/+};RIM1^{fl/+}$	124	834	14.9%	632
$Emx1^{Cre/+};RIM1^{fl/fl}$	53	497	10.7%	386
Totals	**592**	**4307**	**13.7%**	**3491**

No differences in connectivity were found ($p = 0.10$, three-category chi-squared test; $p = 0.19$, Cochran-Armitage test for decreasing trend). $RIM1^{+/+}$ denotes WT, $RIM1\alpha\beta^{fl/fl}$;no-Cre, and $Emx1^{Cre/+};RIM1\alpha\beta^{+/+}$ pooled, as they were not significantly different (328/2233, 53/474, 34/269 respectively, $p = 0.13$, three-category chi-squared test; STAR Methods). For simplicity, and to avoid possible experimenter bias (e.g. slice cutting angle, depth of patching in the slice), only paired recording data from one experimenter (T.A.) was used for this analysis.

Table S2. RIM1αβ KO did not Affect L5 PC Basal Dendrite Spine Densities, Related to Figure 7

Category	Spine density per 10 µm	Number of dendritic segments	Number of cells	Postnatal age
$RIM^{+/+}$	2.9 ± 0.2	45	7	13 ± 0.3
$Emx1^{Cre/+};RIM1^{fl/+}$	2.4 ± 0.1	13	3	12 ± 0
$Emx1^{Cre/+};RIM1^{fl/fl}$	2.7 ± 0.3	12	3	13 ± 0.2

Spine densities were not different ($p = 0.39$, Kruskal-Wallis). Animal ages of this data set were not biased ($p = 0.14$, Kruskal-Wallis). $RIM1^{+/+}$ denotes WT and $Emx1^{Cre/+};RIM1\alpha\beta^{+/+}$ pooled, as they were not different (2.8 ± 0.3 per 10µm, $n = 10$, 3.0 ± 0.2, $n = 12$, $p = 0.67$, Wilcoxon-Mann-Whitney two-sample rank test; STAR Methods).